A First-Principles Model Based on Saturation of the Electron Cyclotron Drift Instability for Electron Transport in Hydrodynamics Simulations of Hall Thruster Plasmas

IEPC-2017-178

Presented at the 35th International Electric Propulsion Conference
Georgia Institute of Technology • Atlanta, Georgia • USA
October 8 – 12, 2017

Alejandro Lopez Ortega[1], Ira Katz[2] and Vernon H. Chaplin[3]
Jet Propulsion Laboratory, California Institute of Technology, Pasadena, CA, 91109, USA

Abstract: We present a computational model based on the hypothesis that the higher-than-expected electron mobility across magnetic field lines observed in Hall thrusters is due to the growth and eventual saturation of the electron cyclotron drift instability. The key improvement of this model with respect to previous work is that it decouples the saturation of the instability from the correlation that exists between mobility and magnitude of the wave perturbations in linear theory, thereby enabling first-principles simulations. The model has been incorporated in the 2-D (r-z) multi-fluids code Hall2De and simulations of the H6 thruster at 300 V, 20 A are numerically stable and achieve a steady-state solution at a computational cost that is not significantly higher than previous Hall2De simulations. The computed location of the acceleration region is found to be within 10% of the length of the acceleration channel compared to that inferred by experiments. The simulations also capture well the plasma gradients along the channel centerline of this thruster. To further establish the validity of this model, we plan to conduct simulations of other thrusters and/or operating conditions.

Nomenclature

$\mathbf{B}$	=	magnetic field
B	=	magnitude of magnetic field
c_s	=	ion sound speed
dV	=	discretized volume in computational grid
dS	=	discretized surface in computational grid
Δt	=	time-step
$\mathbf{E}$	=	electric field
e	=	elementary charge
ε	=	dispersion relation
ε_i	=	imaginary part of dispersion relation
ε_r	=	real part of dispersion relation
ε_0	=	vacuum permittivity
f_s	=	distribution function of species s
F_a	=	anomalous force
$\mathbf{j}_s$	=	current density of species s
k	=	wavenumber modulus

[1] Member of the Technical Staff, Electric Propulsion Group, alejandro.lopez.ortega@jpl.nasa.gov.
[2] Principal Engineer, Propulsion, Thermal, and Material Systems Group, ira.katz@jpl.nasa.gov.
[3] Member of the Technical Staff, Electric Propulsion Group, vernon.h.chaplin@jpl.nasa.gov.

$\hat{\mathbf{k}}$ = direction of wavenumber vector
$\mathbf{k}$ = wavenumber vector
κ = thermal conductivity
λ_{De} = Debye length
$\ln \Lambda$ = Coulomb logarithm
L = length of thruster channel
m = mass
n = number density
$\dot{n}$ = ionization rate per unit volume
$\dot{n}_{CEX}$ = charge exchange rate per unit volume
$\hat{\mathbf{n}}$ = normal vector to mesh edge
N_k = wave action for wavenumber k
$N_{k,sat}$ = wave action at saturation for wavenumber k
N_T = total wave action
Ω_e = Hall parameter
ϕ = plasma potential
$q_{(s)}$ = charge of species s
Q_a = anomalous heating
Q_T = thermal equilibration term in energy equation
$\mathbf{r}$ = position vector
r = radial direction
t = time
T = temperature (in eV)
τ = isotropization time
θ = azimuthal direction
$\mathbf{u}$ = velocity vector
v_{ts} = thermal velocity of species s
v_a = anomalous collision frequency
ω_k = wave frequency
$\omega_{i,k}$ = imaginary part of the wave frequency
$\omega_{i,sat}$ = imaginary part of the wave frequency at saturation
ω_{ie} = linear electron contribution to the imaginary part of the wave frequency
$\omega_{ie,non\text{-}linear}$ = non-linear electron contribution to the imaginary part of the wave frequency
ω_{ii} = ion contribution to the imaginary part of the wave frequency
$\omega_{r,k}$ = real part of the wave frequency
z = axial direction
e = (subscript) electron
i = (subscript) ion
n = (subscript) neutrals
0 = (subscript) first-order term
1 = (subscript) second-order (perturbation) term
$\perp$ = (subscript) direction perpendicular to magnetic field

I.Introduction

Modeling and simulation of the plasma discharge in Hall thrusters play an important role in investigating the physical principles behind the operation of these devices. Numerical methods can also be used for guiding the design of Hall thrusters because one can rapidly modify physical parameters, geometry, and operating conditions. With Hall thrusters being proposed as the main component of the propulsion system of potential deep-space missions, such as ARRM [1-3] and Psyche [4], practical testing of thrusters for their entire operational life becomes increasingly challenging due to time and facility constraints. Numerical simulations can support testing, producing life estimates and providing physical explanations to phenomena observed in the tests.

The most common approach for simulating the plasma conditions in Hall thrusters makes use of a hydrodynamic formulation for modeling the motion of electrons. Moments of Boltzmann's equation for the electron distribution function are integrated over velocity space, resulting in an equation for mass conservation, three equations for tracking the evolution of the momentum, and one energy equation. Due to the low mass of the electrons, the inertia terms are commonly neglected in the momentum equation, the resultant expression being then equivalent to the vector form of Ohm's law. The transport coefficients that appear in Ohm's law, such as the resistivity, are determined under the assumption that the electrons obey a Maxwellian distribution and that classical collisions occur with other species in the plasma, such as neutrals and ions. Simulations that follow this approach have advantages over particle-in-cell (PIC) methods [5-7] (in which a set of hyper-particles representing electrons move in the computational domain according to Lorentz's force). Fluid algorithms produce low levels of noise in the solution and have moderate computational cost, which allow them to be run in hours or days on workstation (or even modern laptop) computers.

Despite the computational advantages of hydrodynamics codes, the implementation of a numerical algorithm fully reliant on physical first-principles has not been possible to date. The reason for this is that classical collision theory predicts resistivity values across magnetic field lines much larger than those required for reproducing the experimentally observed plasma measurements. Historically, numerical and analytical studies have accounted for this phenomenon by introducing an anomalous collision frequency term in the computation of transport coefficients that effectively reduces the Hall parameter. Two-dimensional PIC simulations that do not consistently model the azimuthal drift of the electrons require a similar approach. Other PIC simulations that have self-consistently modeled the electron drift in the azimuthal and either the radial [8] or the axial directions [6, 9] have predicted lower overall resistivity values than those predicted by classical collisions. However, the simplified geometry considered in these simulations makes this approach inapplicable for tasks such as predicting the erosion rates at specific surfaces of the thruster. Kinetic or particle-based simulations in three dimensions are not yet possible, even with the current advancements in computational processing power.

The physical process or processes that facilitate the transport of electrons across magnetic field lines in a Hall thruster are not fully understood. One leading theory, initially proposed by Adam et al. [6], is that the turbulence generated by the electron cyclotron drift instability (ECDI) [10] is the cause of the anomalous electron transport in a Hall thruster. The ECDI is similar to the ion-acoustic instability (IAI) [11-14] in the sense that large electron drift velocities amplify the instability and that the wave frequency is proportional to the ion sound speed. In Hall thrusters, the ExB drift in the azimuthal direction is the suspected source of the instability. The presence of ECDI in Hall thrusters has been confirmed experimentally [15-16], by analysis [16-17], and by means of one-dimensional [18] and two-dimensional [6-9] PIC simulations. The latter have shown enhanced electron transport as the ECDI develops. However, it is still unclear whether the ECDI is the sole (or major) contributor to the anomalous transport of electrons in Hall thrusters.

In this article, we present a physics-based model, based on a pseudo-particle description of ECDI waves , for the computation of the anomalous collision frequency term in Ohm's law's as implemented in our hydrodynamics code Hall2De [19-20]. In Hall2De, a quadrilateral-based computational grid aligned with the magnetic field is employed. A typical simulation domain comprises the acceleration channel and a region of the plume that extends several times the length of the channel in the radial and axial directions. The dimensions of the computational domain enable a realistic simulation of the cathode plume (but not the hollow cathode interior). Cylindrical geometry is assumed, with the axis being the thruster centerline. The equations of motion are solved only in the axial and radial directions. The motion of each species in the plasma is solved separately. The density and velocity distribution of neutral particles is modeled using free-molecular flow, according to a view-factor algorithm described in [21]. Ions are modeled using a hydrodynamics approach that allows for the existence of multiple ion populations, according to their potential and kinetic energy. Density, momentum, and temperature are solved for each of the ion populations. Ionization, charge exchange, and elastic collisions are included. Finally, electrons are modeled using the typical hydrodynamics approach in which inertia terms are neglected. Ohm's law is solved in the directions parallel and perpendicular to the magnetic field lines. The combination of quasi-neutrality, current conservation, and Ohm's law enables the computation of the plasma potential when the anomalous collision frequency term is known or indirectly inferred from experimental measurements. Electron temperature is determined as the solution of the energy conservation equation.

This article is organized as follows. In Section II, we provide a summary of previous efforts to incorporate a self-consistent model of the anomalous collision frequency in Hall2De and comment on the lessons learned from each of those efforts. In Section III, we present a new model that accounts for saturation of the electron cyclotron drift instability. Results of numerical simulations using this model are shown in Section IV. Section V discusses general conclusions about the physics of a Hall thruster that we can draw from the results of our numerical simulations and establishes open questions that warrant further investigation. Section VI summarizes the main findings of this article.

II. Summary of previous efforts to model anomalous electron transport in Hall2De and recent insights on the physics associated with the electron cyclotron drift instability in Hall thrusters

Efforts to self-consistently model the anomalous collision frequency term in Hall2De started in 2015 [22]. The simplified model, based on ion-acoustic instability theory, consisted of an evolution equation for the total wave action, N_T,

$$\frac{\partial N_T}{\partial t} + \nabla \cdot \left(\mathbf{u}_i N_T \right) = 2\omega_i N_T . \quad (1)$$

Linear theory of the ion-acoustic instability determines the imaginary part of the wave frequency (growth rate), ω_i (see Eq. (22,24) for instance). An algebraic relation relates the wave action and the anomalous collision frequency, ν_a,

$$\nu_a \propto \frac{c_s e N_T}{\lambda_{De}^2 \sqrt{m_e m_i} n_0} . \quad (2)$$

where $c_s = \sqrt{eT_e/m_i}$ and $\lambda_{De} = \sqrt{\varepsilon_0 T_e / (e n_0)}$ are the ion sound speed and the electron Debye length, respectively. A similar model was successfully applied to the ion-acoustic instability found in hollow cathode plumes in our OrCa2D code [23-24]. The results produced by the model (1-2) were compared to the anomalous collision frequency in Hall2De's Ohm's law solver, which reproduces plasma measurements. In this paper we label this distribution of the anomalous collision frequency as "experimentally informed" hereinafter. The major difference between self-consistent formulations based on the ion-acoustic instability and the "experimentally informed" distribution occurs in the acceleration region. The quasi-linear IAI theory predicts maximum growth and minimum resistivity for electrons when the electron drift velocity is large. The latter occurs in the acceleration region, characterized by large gradients in the plasma potential in shorts lengths (typically 25% of the thruster channel length). The reason the acceleration region exists in Hall2De simulations is that the "experimentally informed" distribution requires higher resistivity, (i.e. lower anomalous collision frequency) in this region (Fig. 1 for $0.7<z/L<1$) than in the ionization ($z/L<0.7$) or plume ($z/L>1$) regions. If the experimentally informed anomalous collision frequency is replaced by a self-consistent formulation based on the IAI, the acceleration region disappears as the large electron drift almost instantaneously produces growth of the instability and decreasing resistivity. For a fixed electron current, lower resistivity leads in turn to a smooth plasma potential profile along the axial direction that does not resemble the large potential gradients found in the acceleration region of Hall thrusters. This difficulty in reconciling the experimental evidence and the IAI-based model was obvious since our first article [22], in which, in order to obtain acceptable results, we were forced to suppress the growth of the instability inside the acceleration channel.

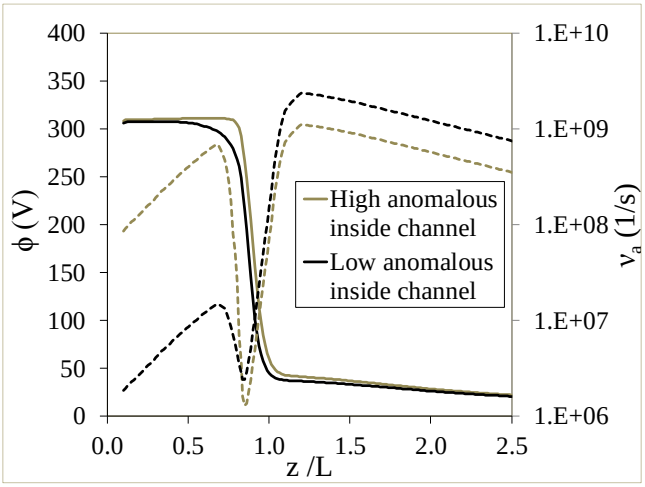

Figure 1. Sensitivity of Hall2De solution to anomalous collision frequency profile along the channel centerline. Note that steep plasma potentials are associated with low values of the anomalous collision frequency (high resistivity) and that the solution upstream of the acceleration region is not very sensitive to large changes in the anomalous collision frequency (comparison between high and low inside channel profiles of the anomalous collision frequency)

In 2016, Mikellides et al. [25] offered additional insight to this problem by solving Eqs. (1-2) backwards, using the experimentally informed profile for v_a to determine the wave action N_T, and finally the growth rate. The growth rate obtained in this manner was then compared to that predicted by linear ion-acoustic instability theory. Results showed that the two growth rates deviated from each other in the acceleration region. It was proposed that Landau damping, a mechanism for which the growth rate of the instability decreases as ions get heated, could explain this discrepancy. It was noted though that predicting the exact contribution of Landau damping was difficult, as the latter is highly sensitive to the ratio of electron and ion temperatures. In the acceleration region, however, the electron temperature appears to be much larger than the ion temperature. Ion temperatures measured by laser-induced fluorescence measurements [26-27] are at most 1 or 2 eV. Thus, the stabilizing effect of Landau damping in the acceleration region is likely small compared to the contribution of the electron drift to the growth of the instability. Inside the channel, as the electron temperature and electron drift decrease, Landau damping may have a more significant effect. However, as shown in Fig. 1, the plasma solution is controlled by the minimum value of the anomalous collision frequency in the acceleration region and is fairly insensitive to changes in the anomalous collision frequency inside the channel.

Katz et al. [28] proposed that the anomalous transport in Hall thrusters is controlled by ion acoustic waves that interact with two distinct ion populations. The first is the main beam, an ion fluid generated upstream of the acceleration region. These ions interact with electrons with the largest ExB drift but it was assumed that the electron drift was completely canceled by Landau damping, using the marginal stability criterion. This assumption increased the resistivity in the acceleration region. The second population is composed of ions generated at low potentials further downstream. Because these ions are not heated and have velocities much different from the main beam ions, it was argued that the amplitude of ion acoustic waves in this population was not Landau-damped and grew to saturation. Scattering from these waves resulted in lower resistivity in the near plume where slow ions make up a significant fraction of the population. While simulations with this model worked in a one-dimensional code, they failed to yield meaningful results when transferred to Hall2De. The main reason for the model not working properly in Hall2De was found to be the the radial motion of plume ions that wasnot captured correctly in the 1-D code.

Lafleur et al. [18] recently performed one-dimensional PIC simulations of the motion of electrons and ions in the azimuthal direction with background conditions similar to those found in Hall thrusters. These simulations offered further insight on the physics of the acceleration region. Saturation of the Electron Cyclotron Drift Instability was observed and it was determined to be caused by ion trapping, a phenomenon where the energy of the ions cannot overcome the amplitude of the plasma potential fluctuations in the waves. It was also noticed that the electron distribution function at saturation was not Maxwellian. In a follow-up article [29], Lafleur et al. employed an equation equivalent to (1) in which it was assumed that the wave action has reached saturation to derive saturation values for the growth rate and resistivity. However, the quantitative values given for the electron resistivity in [18] are an order of magnitude lower than those found in the acceleration zone of Hall thrusters, probably due to the approximations made in the 1-D calculation.

III. First-Principles Model Based on Saturation of the Electron Cyclotron Drift Instability

We apply some of the lessons learned from the work summarized in Section II to the model presented in this paper, which has significant differences with respect to Eq. (1-2). We summarize the key improvements to our model here and describe them in detail in each subsection:

- We no longer use a total wave action equation (Eq. (1)). We solve instead the wave action associated to each member of a discretized space of the wavenumbers that can produce instability. In Eq. (1), the growth rate depends on the wavenumber *k*, which was chosen to be the one that produced the largest growth rate at each point of the computational domain. This approach leads to an overestimation of the total wave action. With the new approach, waves of a certain wavenumber whose amplitude grows at one location of the computational domain can become damped at a different location, independently of the behavior of waves of a different wavenumber. The anomalous collision frequency is computed as a function of the contribution of the wave actions of all wavenumbers.
- We include a non-linear growth rate that becomes zero at wave saturation.
- We substituted Eq. (2) with a model that computes the anomalous collision frequency according to deviations from the Maxwellian distribution function of electrons and ions.
- We included a floor value for the anomalous collision frequency that prevents the drift velocity of electrons from exceeding their thermal velocity.

A. The wave action equation

The plasma wave kinetic equation (c.f. Ref. [13]) for the evolution of a mode of wavenumber k in the plasma is given by

$$\frac{\partial N_k}{\partial t} + \nabla_k \omega_{r,k} \cdot \nabla N_k - \nabla \omega_{r,k} \cdot \nabla_k N_k = 2\omega_{i,k} N_k, \tag{3}$$

where N_k is the wave action, a quantity related to the energy density of a wave as $N_k = W_k/\omega_{r,k}$. $\omega_{r,k}$ and $\omega_{i,k}$ represent, respectively, the real and imaginary part of the wave frequency. The first two terms of the equation model the advection of the wave, the third term accounts for transfer of wave energy between different wavenumbers, and the right-hand side term controls the growth or damping of the wave. Equation (3) is a general expression that can be used to describe the kinetic evolution of any plasma wave. An alternative form of this equation, more appropriate for discretization using a finite volume algorithm is

$$\frac{\partial N_k}{\partial t} + \nabla \cdot \left(N_k \nabla_k \omega_{r,k}\right) - \nabla_k \cdot \left(\nabla \omega_{r,k} N_k\right) = 2\omega_{i,k} N_k. \tag{4}$$

Before we can go further, we need to determine the real and imaginary parts of the wave frequency by computing the dispersion relation.

1. Linear theory for ion-acoustic mode

In order to compute the exact dispersion relation for the ECDI, we need to consider Boltzmann's equation in the presence of an applied magnetic field. However, it has been shown [16] that the ECDI dispersion relation resembles that of the ion-acoustic instability (IAI) but with quantized peaks in the imaginary part of the frequency at wavenumbers that resonate with the cyclotron radius. In the presence of radial perturbations, the quantized peaks disappear and a continuous function that relates the imaginary part of the frequency and the wavenumber is recovered [16]. Thus, we approximate the ECDI dispersion relation to that of the IAI. We follow here the traditional approach of obtaining the dispersion relation from a linear decomposition of the electrostatic Vlasov's equation

$$\frac{\partial f_{(s)}}{\partial t} + \mathbf{u} \cdot \nabla f_{(s)} + \frac{q_s}{m_s} \mathbf{E} \cdot \nabla_{\mathbf{v}} f_{(s)} = 0, \tag{5}$$

into zeroth and first order terms. For simplicity, we have neglected collisions in this formulation but they can be easily included. We make use of the eikonal decomposition for perturbations in the distribution function and electric field:

$$f_{(s)} = f_{0(s)} + \sum_k f_{1k(s)} \exp\left(i\left(\mathbf{k} \cdot \mathbf{r} - \omega_k t\right)\right), \tag{6}$$

$$\mathbf{E} = \mathbf{E}_0 + \sum_k \mathbf{E}_{1k} \exp\left(i\left(\mathbf{k} \cdot \mathbf{r} - \omega_k t\right)\right). \tag{7}$$

The first and second order terms for the plasma potential are then related to the electric field by

$$\begin{aligned} \mathbf{E} &= -\nabla\phi = -\nabla\phi_0 - \sum_k \nabla\phi_{1k} \exp\left(i\left(\mathbf{k} \cdot \mathbf{r} - \omega_k t\right)\right), \\ \phi_{1k} &= \frac{i}{|\mathbf{k}|^2} \mathbf{k} \cdot \mathbf{E}_{1k}. \end{aligned} \tag{8}$$

We then obtain the zeroth-order Vlasov equation:

$$\frac{\partial f_{0(s)}}{\partial t} + \mathbf{v} \cdot \nabla f_{0(s)} + \frac{q_s}{m_s} \mathbf{E} \cdot \nabla_{\mathbf{v}} f_{0(s)} = -\frac{q_s}{m_s} \nabla_{\mathbf{u}} \cdot \left[\sum_k \mathbf{E}_{1k} f_{1k(s)}\right], \tag{9}$$

and a first-order equation that can be decoupled for each *k* value:

$$f_{1k(s)}\left(\omega_k - \mathbf{k}\cdot\mathbf{u}\right) = -\frac{q_s\phi_{1k}}{m_s}\mathbf{k}\cdot\nabla_{\mathbf{u}} f_{0(s)}. \tag{10}$$

We need to assume at this point a shape of the background distribution function. We discuss here the case of a Maxwellian distribution function being employed for ions and electrons,

$$f_{s(0)} = n_{0(s)}\left(\frac{m_s}{2\pi e T_s}\right)\exp\left(-\frac{m_s}{2eT_s}\left(\mathbf{v}-\mathbf{u}_s\right)^2\right), \tag{11}$$

but will comment on the validity of this assumption in different regions of the Hall thruster later. The perturbation density $n_{1k(s)} = \int f_{1k(s)} d\mathbf{v}$ then takes the form:

$$n_{1k(s)} = -\frac{q_s n_{0(s)}\phi_{1k}}{eT_s}\left(1+\zeta_s Z_0\left(\zeta_s\right)\right), \tag{12}$$

with

$$Z_0\left(\zeta_s\right) = i\sqrt{\pi}\exp\left(-\zeta_s^2\right)\left(1+\mathrm{erf}\left(i\zeta_s\right)\right), \quad \zeta_s = \frac{\omega_k - \mathbf{k}\cdot\mathbf{u}_s}{v_s k}, \tag{13}$$

where $v_s = \sqrt{2eT_s/m_s}$. For conditions in the Hall thruster plasma, we typically have $\left|\zeta_e\right| << 1$ and $\left|\zeta_i\right| >> 1$. The latter allows for an asymptotical evaluation of the error function, erf, to yield

$$n_{1k(e)} = \frac{n_{0(e)}\phi_{1k}}{T_e}\left(1+i\sqrt{\pi}\left(\frac{\omega_k - \mathbf{k}\cdot\mathbf{u}_e}{v_e k}\right)\exp\left(-\left(\frac{\omega_k - \mathbf{k}\cdot\mathbf{u}_e}{v_e k}\right)^2\right)\right), \tag{14}$$

$$n_{1k(i)} = -\frac{n_{0(i)}\phi_{1k}}{T_i}\left(-\frac{1}{2}\left(\frac{v_i k}{\omega_k - \mathbf{k}\cdot\mathbf{u}_i}\right)^2 + i\sqrt{\pi}\left(\frac{\omega_k - \mathbf{k}\cdot\mathbf{u}_i}{v_i k}\right)\exp\left(-\left(\frac{\omega_k - \mathbf{k}\cdot\mathbf{u}_i}{v_i k}\right)^2\right)\right). \tag{15}$$

To obtain the dispersion relation, we relate perturbations in the plasma potential and the density of electrons and ions through Poisson's equation

$$0 = 1 - \frac{1}{\varepsilon_0 k^2 \phi_{1k}}\sum_s q_s n_{1(s)} = \varepsilon(\mathbf{k},\omega_k). \tag{16}$$

Under the assumption that the imaginary part is small compared to the real part of the frequency $\omega_{r,k} >> \omega_{i,k}$, we can linearize (16) to decouple the dispersion relation into two equations that allow us to solve for the real and imaginary components of the frequency, respectively,

$$0 = \varepsilon(\mathbf{k},\omega_k) = \varepsilon_r(\mathbf{k},\omega_{r,k}) + i\left(\varepsilon_i(\mathbf{k},\omega_{r,k}) + \omega_{i,k}\frac{\partial\varepsilon_r(\mathbf{k},\omega_{r,k})}{\partial\omega_k}\right). \tag{17}$$

We first solve for

$$0 = \varepsilon_r(\mathbf{k}, \omega_{r,k}) = 1 - \frac{e}{\varepsilon_0 k^2 \phi_k}\left(\mathrm{Re}\left[n_{1k(i)}\right] - \mathrm{Re}\left[n_{1k(e)}\right]\right), \tag{18}$$

which can be written, assuming quasi-neutrality of the background plasma, $n_0 = n_{0(e)} = n_{0(i)}$, as

$$0 = 1 + \frac{n_o e}{\varepsilon_0 k^2 T_e}\left(-\frac{eT_e k^2}{m_i\left(\omega_{r,k} - \mathbf{k}\cdot\mathbf{u}_i\right)^2} + 1\right). \tag{19}$$

This equation can be solved for $\omega_{r,k}$, yielding,

$$\omega_{r,k} = \mathbf{k}\cdot\mathbf{u}_i \pm \frac{c_s}{\sqrt{1 + k^2\lambda_{De}^2}}. \tag{20}$$

We proceed to determine the imaginary part of the frequency using (17). We first take the intermediate step to compute the derivative of the real part of the dispersion relation with respect to the frequency,

$$\frac{\partial \varepsilon_r\left(\omega_{r,k}, \mathbf{k}\right)}{\partial \omega_k} = \pm\frac{2e^2 n_0\left(1 + k^2\lambda_{De}^2\right)^{3/2}}{\varepsilon_0 m_i c_s^3 k^3}. \tag{21}$$

The latter expression will be used multiple times in the derivation of our model. Finally, the imaginary part of the instability can be written as the contribution of ion and electron perturbations,

$$\omega_{i,k} = \omega_{ii} + \omega_{ie} = \frac{e}{\varepsilon_0 k^2 \phi_k}\frac{\mathrm{Im}\left[n_{1k(i)}\right] - \mathrm{Im}\left[n_{1k(e)}\right]}{\dfrac{\partial \varepsilon_r(\mathbf{k}, \omega_r)}{\partial \omega}}. \tag{22}$$

It will be useful in our formulation to write the imaginary part of the electron and ion perturbation densities in terms of their contribution to the imaginary part of the wave frequency,

$$\begin{aligned}
\mathrm{Im}\left[n_{1k(e)}\right] &= -\frac{2n_0 e\left(1 + k^2\lambda_{De}^2\right)^{3/2}}{m_i c_s^3 k}\phi_{1k}\omega_{ie}, \\
\mathrm{Im}\left[n_{1k(i)}\right] &= -\frac{2n_0 e\left(1 + k^2\lambda_{De}^2\right)^{3/2}}{m_i c_s^3 k}\phi_{1k}\omega_{ii}.
\end{aligned} \tag{23}$$

For Maxwellian electrons and ions, the electron and ion contributions take the form, respectively,

$$\begin{aligned}
\omega_{ie} &= \frac{\sqrt{\pi} c_s k}{2\left(1 + k^2\lambda_{De}^2\right)^{3/2}}\left(\pm\left(\frac{\mathbf{k}\cdot\left(\mathbf{u}_e - \mathbf{u}_i\right)}{v_e k} \mp \frac{c_s}{v_e\left(1 + k^2\lambda_{De}^2\right)^{1/2}}\right)\exp\left(-\left(\frac{\mathbf{k}\cdot\left(\mathbf{u}_e - \mathbf{u}_i\right)}{v_e k} \mp \frac{c_s}{v_e\left(1 + k^2\lambda_{De}^2\right)^{1/2}}\right)^2\right)\right), \\
\omega_{ii} &= -\frac{\sqrt{\pi} c_s k}{2\left(1 + k^2\lambda_{De}^2\right)^{3/2}}\left(\frac{T_e}{T_i}\left(\frac{c_s}{v_i\left(1 + k^2\lambda_{De}^2\right)^{1/2}}\right)\exp\left(-\left(\frac{c_s}{v_i\left(1 + k^2\lambda_{De}^2\right)^{1/2}}\right)^2\right)\right) - \frac{\nu_{in}}{2},
\end{aligned} \tag{24}$$

where we have included the ion-neutral collision term, ν_{in}, that had been previously neglected in Vlasov's equation (9). Note that the maximum growth of the instability occurs when the wavevector **k** is collinear with the relative drift

between electrons and ions. For the negative branch of the solution, **k** must be in the opposite direction of the drift. Since the electron drift in the azimuthal direction is much larger than all the other components of the electron and ion velocity, we can assume that the wave energy associated with wavevectors aligned with the azimuthal direction is dominant. In that case, $\mathbf{u}_i \cdot \mathbf{k} \approx 0$ and the two branches of the solution behave in the same manner for **k** of opposite direction. For convenience, we will write our equations assuming that **k** has the same direction as $\mathbf{u}_e$-$\mathbf{u}_i$ (i.e., choosing the positive branch of the solution).

2. Simplification of the wave action equation

We can make use of cylindrical coordinates (r, θ, z), expressions (20, 22, 24), and certain assumptions about the electron cyclotron drift instability to simplify (4). $\omega_{r,k}$ is a function of the background plasma quantities and the wavenumber. Background plasma quantities do not vary in the azimuthal direction. We also assume that $N_k \approx N_k(\mathbf{r}, k_\theta)$ and $k \approx k_\theta$ based on our discussion in the previous paragraph. The third term in (4) then becomes

$$\nabla_k\left(N_k \nabla \omega_r\right) = N_k \nabla \cdot \mathbf{u}_i + \frac{k u_{r,i}}{r}\frac{\partial N_k}{\partial k}. \tag{25}$$

The second term on the right-hand side represents the transfer of energy between waves, which in the case of purely azimuthal waves only occurs when ions have radial velocities. We neglect this term since the direction of the iopn flow in Hall thruster channels is predominantly axial. The transfer of wave energy between wavenumbers have already been considered in our assumption that the dispersion relation is similar to the continuous spectrum of the IAI instead of the quantized spectrum of the ECDI. The first term on the right-hand side of (25) allows us to rewrite Eq. (4) in the form of an advection equation with a source term:

$$\frac{\partial N_k}{\partial t} + \mathbf{u}_i \cdot \nabla N_k = 2\omega_{i,k} N_k. \tag{26}$$

In Hall2De, this equation is written in conservative form and discretized by means of finite volumes. We use an implicit scheme for time discretization, the chain rule, and Gauss' theorem to write

$$\frac{1}{\Delta t}\left(\int_V N_k^{t+\Delta t} dV - \int_V N_k^t dV\right) + \int_{\Delta V} N_{k,upw}^{t+\Delta t}\mathbf{u}_i \cdot \hat{\mathbf{n}} dS = \int_V \left(2\omega_{i,k} + \nabla \cdot \mathbf{u}_i\right) N_k^{t+\Delta t} dV. \tag{27}$$

$N_{k,upw}^{t+\Delta t}$ is the wave action of the upwind cell, determined by the direction of $\mathbf{u}_i$ with respect to the normal to the surface, $\hat{\mathbf{n}}$. We also discretize the wavenumber space, solving for individual wave actions associated to each wavenumber. Lower and upper bounds to the wavenumber spectrum can be found by examination of the background plasma solution. In particular, we know from (24) that the maximum growth rate is obtained for $k = 1/\sqrt{2\lambda_{De}^2}$, assuming that the ion contribution to the imaginary part of the frequency (Landau damping) is negligible. If Landau damping is not negligible, the maximum growth rate is found for values of $k < 1/\sqrt{2\lambda_{De}^2}$. Since we neglected the second term in (25), we can solve for each wave number independently of the others. The implementation of this system of partial differential equations in Hall2De has a similar computational cost as solving for the ion motion when a moderate (10 to 20) number of different wavenumbers are considered.

3. Saturation mechanism and implementation in wave action equation

Assuming that electrons and ions obey a Maxwellian distribution function, the imaginary part of the frequency (22,24) does not saturate except in the strange case of $\omega_{ie} = -\omega_{ii}$. With this approach, we cannot capture saturation

caused by non-linear effects that emerge when the perturbation amplitude becomes large enough. As a first approximation, we can rewrite the imaginary part of the frequency to account for saturation as,

$$\omega_{i,k,sat} = \omega_{i,k,linear}\left(1-\frac{N_k}{N_{k,sat}}\right), \tag{28}$$

where $\omega_{i,k,linear}$ is given by (22,24). The wave action equation now reads

$$\frac{\partial N_k}{\partial t} + \mathbf{u}_i \cdot \nabla N_k = 2\omega_{i,k,sat} N_k. \tag{29}$$

Recent PIC simulations by LaFleur [18] have shown that ion trapping is a likely mechanism to explain wave saturation. We will explore this possibility here, imposing the condition that the potential perturbation amplitude cannot exceed the energy level associated with the ion sound speed:

$$\phi_{1k}^{sat} = \frac{m_i}{2e}\left(\frac{\omega_r}{k}\right)^2 \approx \frac{T_e}{2\left(1+k^2\lambda_{De}^2\right)}. \tag{30}$$

The perturbation potential is related to the wave action by definition as

$$N_k \equiv \frac{\varepsilon_0 k^2 \phi_{1k}^2}{2e}\frac{\partial \varepsilon_r(\mathbf{k},\omega_r)}{\partial \omega} = \frac{e n_0 \left(1+k^2\lambda_{De}^2\right)^{3/2}}{m_i c_s^3 k}\phi_{1k}^2, \tag{31}$$

where we have made use of (21). Using (30-31), we obtain the value of the saturation wave action:

$$N_{k,sat} = \frac{n_0 T_e}{4c_s k\left(1+k^2\lambda_{De}^2\right)^{1/2}}. \tag{32}$$

B. Anomalous collision frequency

We use Eq. (29) to determine the wave action at each point of the Hall2De computational domain. However, in order to bring closure to the hydrodynamics equations in Hall2De, we need to relate the wave action to zeroth-order effects in the background plasma solution. Taking the first moment of Boltzmann's equation for electrons in the presence of a magnetic field, classical collisions, and wave perturbations, we obtain

$$0 = -n_0 e\mathbf{E} - n_0 e\mathbf{u}_e \times \mathbf{B} - \nabla\left(e n_0 T_e\right) - n_0 m_e\left[\left(\nu_{ei}\right)\left(\mathbf{u}_e - \mathbf{u}_i\right) + \nu_{en}\mathbf{u}_e\right] + \mathbf{F}_{a(e)}, \tag{33}$$

where **B** is the magnetic field, and ν_{ei} and ν_{en} are the electron-ion and electron-neutral classical collision frequencies, respectively. We have also neglected the inertia terms and assumed that the neutral velocity is negligible (i.e., $\mathbf{u}_e >> \mathbf{u}_n$). $\boldsymbol{F}_{a(e)}$ represents the anomalous force due to wave perturbations and, following the approach used in (9), can be written as

$$\mathbf{F}_{a(e)} = \frac{e}{N}\int \mathbf{v}\nabla_{\mathbf{v}} \cdot \left[\sum_k \mathbf{E}_{1k} f_{1k(e)}\right] d\mathbf{v} = \frac{e}{N}\sum_k \mathbf{k}\phi_{1k}\,\mathrm{Im}\left[n_{1k(e)}\right], \tag{34}$$

where N is the number of wavenumbers in the discretized space used for the computations. We would like to express the anomalous force in terms of an anomalous collision frequency so it can be combined with the electron-ion and electron-neutral collision frequencies. We write

$$\mathbf{F}_{a(e)} = -m_e n_0 \nu_a\left(\mathbf{u}_e - \mathbf{u}_i\right), \tag{35}$$

With the anomalous collision frequency being,

$$\nu_a = -\frac{e}{Nm_e n_0 \left|\mathbf{u}_e - \mathbf{u}_i\right|^2} \sum_k \left(\mathbf{u}_e - \mathbf{u}_i\right) \cdot \mathbf{k} \phi_{1k} \, \mathrm{Im}\left[n_{1k(e)}\right] \approx -\frac{e}{Nm_e n_0 \left|\mathbf{u}_e - \mathbf{u}_i\right|} \sum_k k \phi_{1k} \, \mathrm{Im}\left[n_{1k(e)}\right] \quad (36)$$

We have assumed again here that the wavevector is collinear with the relative drift velocity between electrons and ions. Making use of (24), we can relate the anomalous collision frequency to the wave action

$$\nu_a = \frac{e^2}{Nm_e n_0 \left|\mathbf{u}_e - \mathbf{u}_i\right|} \sum_k k \phi_{1k}^2 \frac{2n_0 \left(1 + k^2 \lambda_{De}^2\right)^{3/2}}{m_i c_s^3} \omega_{ie} = \frac{2e}{Nm_e n_0 \left|\mathbf{u}_e - \mathbf{u}_i\right|} \sum_k k N_k \omega_{ie}. \quad (37)$$

For the case of Maxwellian electrons, we can simplify this expression assuming that $c_s << \left|\mathbf{u}_e - \mathbf{u}_i\right|$. We also take into account that $\nu_e >> \left|\mathbf{u}_e - \mathbf{u}_i\right|$ (which is a condition for $\zeta_e = \left(\omega - \mathbf{k} \cdot \mathbf{u}_e\right)/\left(\nu_e k\right) << 1$ in (12-13)) to arrive at the value of the anomalous collision frequency as a function of the wave action for quasi-linear IAI theory:

$$\nu_a = \frac{\sqrt{\pi} c_s e}{N\sqrt{2m_e m_i} n_0} \sum_k N_k \frac{k^2}{\left(1 + k^2 \lambda_{De}^2\right)^{3/2}}. \quad (38)$$

A key assumption is our model is that the distribution function for electrons may not be Maxwellian in all regions of the computational domain. If this is the case, Eq. (24) for electrons is no longer valid and the anomalous collision frequency cannot be related to the wave action by (38). If the electron distribution function is not Maxwellian, we can still compute Im[$n_{1k(e)}$] indirectly. We combine Eq. (22) and (28) to write

$$\omega_{i,k} = \omega_{i,k,sat} = \omega_{i,k,linear} \left(1 - \frac{N_k}{N_{k,sat}}\right) = \frac{e}{\varepsilon_0 k^2 \phi_k} \frac{\mathrm{Im}\left[n_{1k(i)}\right] - \mathrm{Im}\left[n_{1k(e)}\right]}{\frac{\partial \varepsilon_r(\mathbf{k}, \omega_r)}{\partial \omega}}. \quad (39)$$

We need to assume that we know ω_{ii} in order to determine $\mathrm{Im}\left[n_{1k(e)}\right]$,

$$\mathrm{Im}\left[n_{1k(e)}\right] = -\frac{2en_0 \left(1 + k^2 \lambda_{De}^2\right)^{3/2} \phi_k}{m_i c_s^3 k} \left(\omega_{i,k,sat} - \omega_{ii}\right). \quad (40)$$

This equation computes a generalized contribution of the electrons to the imaginary part of the wave frequency as $\omega_{i,k,sat}$-ω_{ii}. If we know ions are Maxwellian, then we can use ω_{ii} from (24). However, we assumed in (30) that saturation occurs due to ion trapping, a mechanism that will produce deviations from a Maxwellian distribution for ions. Since we cannot quantify the effect of ion trapping on ω_{ii}, we acknowledge this limitation of the model and will comment further on this topic as we present results in Sections IV and V. Even though the distribution function that the electrons adopt as the waves approach saturation remains unknown, the model predicts that the contribution of the electrons to the growth of the instability decreases near saturation. Note that if the wave action is far from its saturation value then $\omega_{i,k,sat} - \omega_{ii} \approx \omega_{ie}$. Using (40), we then write the anomalous collision frequency in a general form that depends on whether the distribution function for the electrons and ions is Maxwellian or not:

$$\nu_a = \frac{2e}{Nm_e n_0 \left|\mathbf{u}_e - \mathbf{u}_i\right|} \sum_k k N_k \left(\left(1 - f\right)\omega_{ie} + f\left(\omega_{i,k,sat} - \omega_{ii}\right)\right) = \frac{2e}{Nm_e n_0 \left|\mathbf{u}_e - \mathbf{u}_i\right|} \sum_k k N_k \omega_{ie,non-linear}, \quad (41)$$

where f is a function of the background plasma properties that will be determined in Subsection II D.

We also impose a floor on the anomalous collision frequency, which is given by the condition that the electrons cannot exceed the thermal speed:

$$\sqrt{\frac{2eT_e}{m_e}} \geq \frac{j_{e\theta}}{en_0} = \Omega_e \frac{j_{e\perp}}{en_e} = \frac{eB}{m_e\left(\nu_{ei}+\nu_{en}+\nu_a\right)}\frac{j_{e\perp}}{en_0}, \tag{42}$$

where $j_{e\perp}$ is the electron current density perpendicular to the magnetic field lines and Ω_e is the Hall parameter. The floor value for the anomalous collision frequency then becomes

$$\nu_{a,floor} = \frac{B}{m_e n_0}\frac{j_{e\perp}}{\sqrt{2eT_e/m_e}} - \nu_{ei} - \nu_{en}. \tag{43}$$

The floor anomalous collision frequency can be interpreted as a simplified variable that accounts for the existence of other kinetic instabilities that prevent the electron drift from exceeding the electron thermal speed. These effects cannot be modeled based on the simplified theory of the ECDI presented here, which assumes $|\mathbf{u}_e| << v_{te}$ at all times, and may indeed involve other mechanisms that exhibit smaller time-scales, such as the two-stream instability of electrons and the Buneman instability.

C. Anomalous heating

We can determine the electron and ion temperatures by taking the second moment of Boltzmann's equation. It was shown in [24] that the effect of plasma waves in the heating of electrons in negligible. For ions, however, anomalous heating cannot be neglected. The ion internal energy equation takes the form

$$\frac{3}{2}e\frac{\partial\left(n_0T_i\right)}{\partial t} + \nabla\cdot\left(\frac{3}{2}en_0T_i\mathbf{u}_i - \kappa_i\nabla T_i\right) + en_0T_i\cdot\nabla\left(\mathbf{u}_i\right) = Q_i^T + \left(\dot{n}+\dot{n}_{CEX}\right)\left(\mathbf{u}_i-\mathbf{u}_n\right)^2 + Q_{a(i)}, \tag{44}$$

with κ_i the ion thermal conductivity, Q_i^T a volumetric heating term that accounts for thermal equilibration between different species in the plasma, and $\dot{n}$ and $\dot{n}_{CEX}$ the generation rate of ions due to ionization and charge exchange per unit volume. Following the approach of (9) and (34), we find the heating produced by anomalous effects can be quantified as

$$Q_{a(i)} = -\frac{e}{2N}\int u^2\nabla_{\mathbf{u}}\cdot\left[\sum_k \mathbf{E}_{1k}\, f_{1k(i)}\right]d\mathbf{u} = -\frac{e}{N}\sum_k \phi_{1k}\,\mathrm{Im}\left[\omega_k n_{1k(i)}\right]. \tag{45}$$

Without losing any generality, we can rewrite the anomalous heating of ions in terms of known quantities making use of (18, 24, 39)

$$Q_{a(i)} = -\frac{e}{N}\sum_k \phi_{1k}\left(\omega_{r,k}\,\mathrm{Im}\left[n_{1k(i)}\right] + \omega_{i,sat}\,\mathrm{Re}\left[n_{1k(i)}\right]\right) = \frac{1}{N}\sum_k \frac{ec_skN_k}{\left(1+k^2\lambda_{De}^2\right)^{1/2}}\left(2\omega_{ii}+\omega_{i,k,sat}\right). \tag{46}$$

D. A physics-based model to determine deviations from the Maxwellian distribution function of electrons

We need to determine the form of the function *f* in (41) to bring closure to our model. We first note that Eq. (40) is general enough to always hold when ions are Maxwellian. We can determine the regions of the thruster in which

the ions remain Maxwellian by comparing the equilibration time of ions, τ_{ii}, with the characteristic length of the thruster channel L and the ion velocity. We define the non-dimensional number

$$K_i = \frac{L}{\tau_{ii}|\mathbf{u}_i|}. \tag{47}$$

The equilibration time for ions is defined as

$$\tau_{ii} = \frac{12\pi^{3/2}\varepsilon_0^2\sqrt{m_i}(eT_i)^{3/2}}{n_0 e^4 \ln\Lambda}, \tag{48}$$

with ln Λ the Coulomb logarithm. Thus, $f \approx 1$ when $K_i >> 1$. In order to determine whether electrons constitute a Maxwellian distribution, we compare the isotropization time for electrons with the velocity of the electrons perpendicular to the magnetic field and the characteristic length of the thruster,

$$K_e = \frac{en_0 L}{|j_\perp|\tau_{ee}}, \tag{49}$$

with the isotropization time τ_{ee} being computed as

$$\tau_{ee} = \frac{\varepsilon_0^2\sqrt{m_e}(eT_e)^{3/2}}{2\sqrt{\pi}n_0 e^4 \ln\Lambda} A^2\left[-3+(A+3)\frac{\tan^{-1}\left(A^{1/2}\right)}{A^{1/2}}\right]^{-1}. \tag{50}$$

The coefficient A is the ratio of the energy of the electrons in the azimuthal and the cross-field directions

$$A = \frac{m_e}{2eT_e}\left(\frac{\Omega_e j_\perp}{en_0}\right)^2. \tag{51}$$

When ions are Maxwellian or electrons are not Maxwellian, $f \approx 1$. Conversely, $f \approx 0$ only when electrons are Maxwellian and ions are not. Thus, we can define f as

$$f = \{(1-\exp(-K_i))+(\exp(-K_e))(\exp(-K_i))\}. \tag{52}$$

This formulation captures the electron contribution to the imaginary part of the frequency when at least one of the species, electrons or ions, follows a Maxwellian distribution. When neither distribution is Maxwellian, $f \approx 1$. If at the same point at which the latter happens, $N_k \approx N_{k,sat}$, we have $\omega_{i,k,sat} \approx 0$ and the anomalous collision frequency will read as

$$\nu_a = -\frac{2e\omega_{ii}}{m_e n_0|\mathbf{u}_e - \mathbf{u}_i|}\sum_k kN_k. \tag{53}$$

However, ω_{ii} as given by (24) is only applicable to Maxwellian ions. It will be shown in the next sections that only in the acceleration region the distribution functions for ions and electrons are not Maxwellian and $N_k \approx N_{k,sat}$. The anomalous collision frequency is then controlled by the floor anomalous collision frequency (43).

IV. Simulations of the H6 thruster with first-principles model of anomalous transport

The numerical simulations in this article are conducted with the computational model of the H6 thruster. The H6 is a 6 kW-class thruster developed in a joint effort of the University of Michigan, the Air Force Research Laboratory (AFRL) and the Jet Propulsion Laboratory (JPL) [30-31]. It features a centerline-mounted cathode and is designed for nominal operation at 300 V, discharge current of 20 A, and 20 mg/s flow rate. Under these conditions, 400 mN of thrust and a specific impulse of approximately 1950 s are achieved. In order to explore the possible effects of Landau damping [25], two simulations were conducted. In the first simulation ("cold ions simulation"), we did not solve for the ion energy equation (44) and instead used a fixed ion temperature of 0.05 eV, which would prevent any significant Landau damping. In the second simulation ("warm ions simulation"), we made use of (44) to compute the ion temperature. We only considered singly charged ions in these simulations. We do not expect significant changes in the physics if multiply charged ions are included in the simulations since singly charged ions account for approximately 80% of the total ions in the beam. Simulations were conducted at the nominal operating conditions and initiated using the experimentally informed profile of the anomalous collision frequency until reaching steady state. At this point, the first-principles model was initiated with no blending period for transitioning between the experimentally informed and first-principles models. The first-principles model used 10 discrete wavenumbers between 500 m^{-1} and 5000 m^{-1}. We impose as initial condition for the wave action values that are ten orders of magnitude lower than the saturation wave action (32). During the transitory that occurs after the first-principles model is turned on, we had to impose f=0 in Eq. (41) for locations downstream of the peak magnetic field to avoid large fluctuations in the plasma that prevented the solution from reaching steady state. After the solution reached steady state, we removed such condition, an action that did not affect the solution. We also included a multiplying factor for the floor anomalous collision frequency (43). The value of this coefficient was determined so the discharge current in the simulations is exactly 20 A. We found that a value of 1.3 for the multiplying factor was needed. If the factor was set to exactly 1, the discharge current was slightly lower than 19 A. We consider the fact that the multiplying factor is order unity remarkable given that the floor anomalous collision frequency is actually a very simplified representation of the physics that may occur in the acceleration region, where electrons and ions do not obey Maxwellian distribution functions. In the subsections below, we discuss in detail the results of the two simulations.

A. Wave action and saturation of the instability

Figure 2 depicts the steady state solution of Eq. (29) for the simulations with cold and warm ions, respectively. We have chosen to plot a representative subset of the 10 discrete wavenumbers used in the simulations. In the legend, k=i, represents the solution for the i-th wavenumber in the simulation. We can recover k (in m^{-1}) multiplying i by 500. The wave action values at saturation, Eq. (32), for each wavenumber are plotted as dotted lines. In the case of cold ions, the Landau damping term (ω_{ii} in Eq. (24)), is negligible and saturation of the wave action occurs at almost all locations along the channel centerline. Next to the anode (z/L<0.5), the wave action becomes slightly lower than its saturation value due to the presence of ion-neutral collisions. In the warm-ions simulation, the effect of Landau damping is only noticeable for z/L<0.5. Except for the first wavenumber, waves are damped in the first half of the channel. After the channel midpoint, Landau damping becomes negligible compared to the electron drift contribution to the instability and the wave action values quickly reach their saturation value. In order to understand why Landau damping becomes negligible after the midpoint, Fig. 3 depicts the 2-D distribution of the ion temperature inside the channel. This temperature has been computed taking into account anomalous heating. The ion temperature is, on average, approximately 0.5 eV inside the channel. In the acceleration region, the ion temperature decreases due to adiabatic cooling (term $en_0 T_i \cdot \nabla(\mathbf{u}_i)$ in (44)). This distribution of the ion temperature in the channel does not suggest that ion trapping occurs as heating from the waves is not enough to bring the ion temperature close to the electron temperature (see, for instance, Fig. 8). For the same reason, Landau damping, which according to (24) increases as the ratio of the electron and ion temperatures decreases, should not be significant. However, the ion distribution function ceases to be Maxwellian in the acceleration region (see Fig. 5) and the ion temperature, which is computed assuming hydrodynamics equations, may not be meaningful for regions of K_i<<1. For the first wavenumber, Landau damping appears not to have an effect. In order to understand this result, we need to interrogate Eq. (29) with the help of Fig. 4. In Fig. 4 (left-bottom), we depict three values of the imaginary part of the wave frequency along the channel centerline. The first and second values in the legend are $\omega_{i,k,linear}$ and $\omega_{i,k,sat}$ in Eq. (28), respectively. The third value is the contribution of the electrons to the imaginary part of the frequency ($\omega_{ie,non-linear}$ in Eq. (41)). For z/L<0.5, the linear growth rate $\omega_{i,k,linear}$ is negative due to Landau damping and the velocity vector $\mathbf{u}_i$ is towards the anode. In this region of the channel, according to Eq. (29), the wave action will grow if the rate at which wave action is advected is

larger than the damping rate. The Landau damping term (ω_{ii} in Eq. (24)) increases with k (for instance, compare $\omega_{i,k,linear}$ for the first and ninth wavenumbers in Fig. (4)). Since $\mathbf{u}_i$ in the axial direction is negative, the advection term transports the wave action from locations in which the Landau damping is lower. Thus, for the first wavenumber, the advection is larger than the damping and the wave grows and eventually saturates even when Landau damping is present. For the ninth wavenumber, the damping rate is higher than the advection rate and the wave action associated to this wavenumber does not grow for $z/L<0.5$.

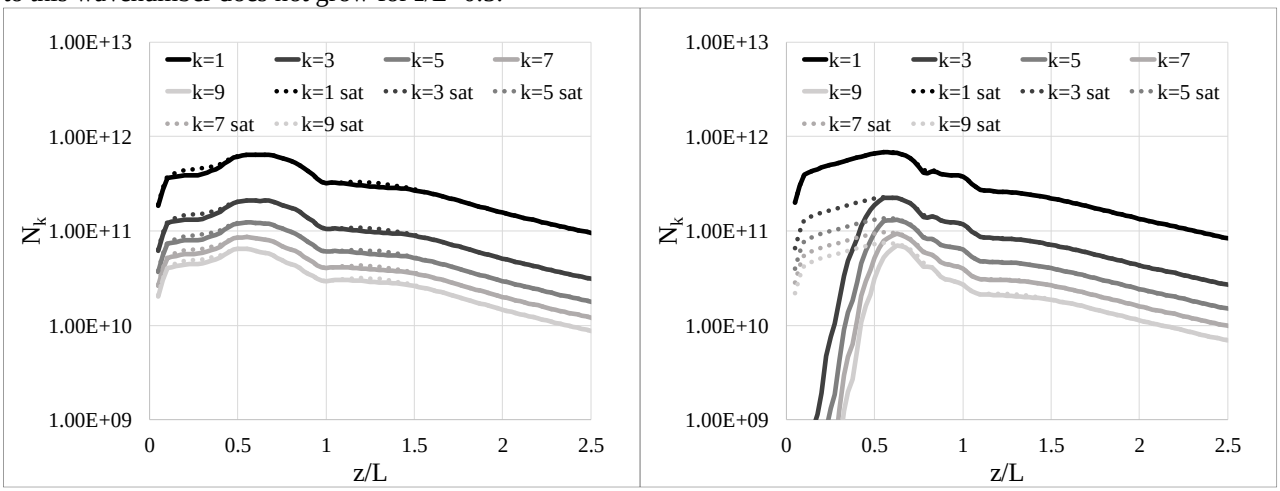

Figure 2. Wave action for multiple wavenumbers and comparison with saturation wave action (32). In the legend k=i, with i being the i-th wave number in the simulation, the wavenumber in m^{-1} units can be obtained multiplying i by 500. Left: cold ions simulation, right: warm ions simulation.

We can gain additional insight on the behavior of our first-principles model by looking at the results depicted in Fig. 4 and Fig. 5. Figure 4 shows the evolution of the terms $\omega_{i,k,linear}$ and $\omega_{i,k,sat}$ in Eq. (28), and the contribution of the electrons to the imaginary part of the frequency ($\omega_{ie,non-linear}$ in Eq. (41)) for the first and ninth wavenumbers of each of the simulations. Since the plots are in logarithmic scale, the absolute values when variables are negative are plotted as dotted lines. Figure 5 depicts the 2-D contour plot of the coefficients K_e (49) and K_i (47) used to compute f (52). Starting with the cold-ions simulation (upper row), we observe that the linear growth rate is maximum in the acceleration region. However, due to saturation of the instability (Fig. 2), we only find two segments with $\omega_{i,k,sat} > 0$, which are located at $z/L<0.5$ and $1<z/L<1.5$. These segments correspond to the locations in Fig. 2 for which the wave action is slightly lower than the saturation value. Thus, the saturation model completely masks the fact that the growth rate predicted by linear theory is maximum at the acceleration region. The maximum linear growth rate predicted for the ninth wavenumber is larger than for the first wavenumber. This is due to the ninth wavenumber being closer to the theoretical maximum growth rate in the acceleration region, which occurs for $k^2\lambda_{De}^2 = 1/2$. However, since the Debye length varies along the channel centerline, the linear growth rate for the ninth wavenumber exhibits a sudden decrease in value downstream of its maximum. This is due to $k^2\lambda_{De}^2 > 1/2$ for the ninth wavenumber in the vicinity of the maximum value of the Debye length (at approximately $z/L=1$). For the first wavenumber, $k^2\lambda_{De}^2 << 1/2$ at all times. The contribution of electrons to the imaginary part of the frequency is given by $(1-f)\omega_{ie} + f(\omega_{i,k,sat} - \omega_{ii})$. Since Landau damping is negligible for cold ions, the latter expression can be approximated, making use of (24), as $(1-f)\omega_{i,k,linear} + f\omega_{i,k,sat} + \nu_{in}/2$. According to the definition of f in (52), $f=0$ when K_e is large and K_i small. The latter only occurs in the plume region ($z/L>1$). As shown in Fig. 4, for $z/L>1$, the electron contribution equals the linear growth rate. Inside the channel, $f\sim1$ and the electron contribution to the imaginary part of the frequency decreases by more than an order of magnitude with respect to its value in the plume and by more than three orders of magnitude with respect to the value predicted by linear theory.

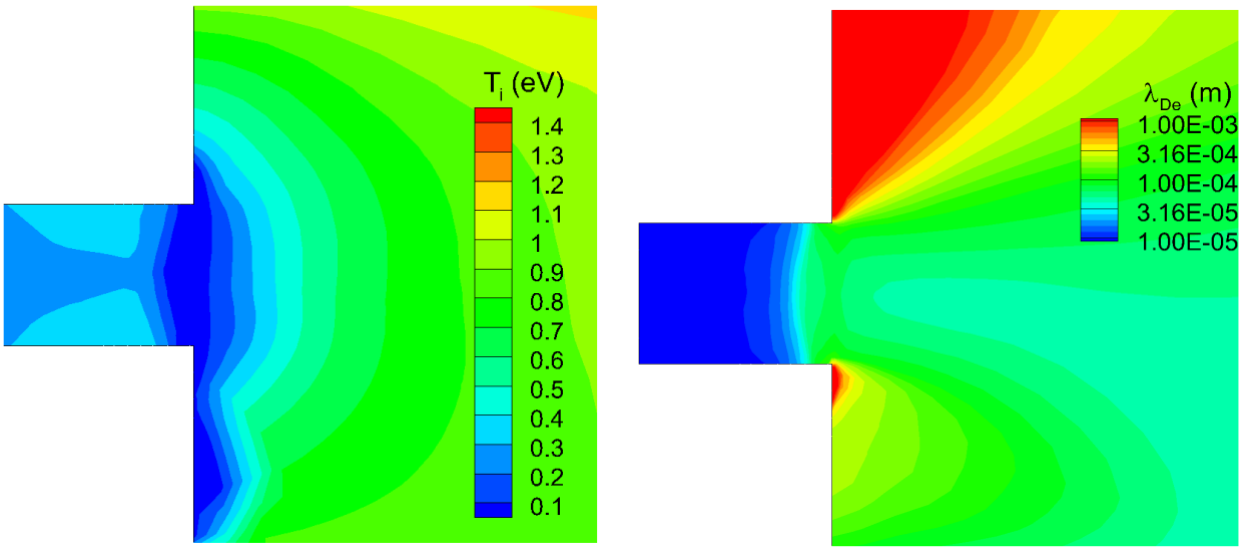

Figure 3. 2-D contour plot of the ion temperature (left) and Debye length (right) for the warm-ions simulation

For the simulation with warm ions (second row of Fig. 4), we encounter qualitatively similar results. A major difference is that the linear growth rate is only positive for $z/L>0.6$ due to Landau damping affecting the solution close to the anode. As in the cold-ions simulation, the ninth wavenumber exhibits a larger value of the maximum linear growth rate than the first wavenumber. This maximum is followed by a rapid shift to a negative growth rate at approximately $z/L=1$. This is due to the Debye length having a larger effect in the warm-ions simulation because the term $1+k^2\lambda_{De}^2$ effectively decreases the ratio T_e/T_i in the exponential term of Eq. (24). For the first wave-number $k^2\lambda_{De}^2 << 1$ and the linear growth rate has a smooth behavior in the acceleration region. As expected, $\omega_{i,k,sat}$ for the ninth wavenumber is negative for $z/L<0.6$ and approaches $\omega_{i,k,linear}$ since $N_k<<N_{k,sat}$. For the first wavenumber, $\omega_{i,k,sat}$ is only positive in one segment between $z/L=0.7$ and $z/L=0.75$ and zero elsewhere. The value of the saturation growth rate in this segment is approximately two orders of magnitude lower than the linear growth rate, which suggests that the ratio $N_k/N_{k,sat}\sim0.99$. Such small differences between the wave action and its saturation value cannot be resolved in the plot shown in Fig. 2. The electron contribution to the imaginary part of the wave frequency follows a behavior similar to the cold-ions simulation in the plume, where $f=0$. Inside the channel however, Landau damping is not negligible, which implies that when $f=1$, the electron contribution is $\omega_{i,k,sat}-\omega_{ii}$ (note that $\omega_{ii}<0$). The electron contribution to the growth rate inside the channel is then larger than in the cold-ions simulation since the magnitude of ω_{ii} increases when ions are warmer.

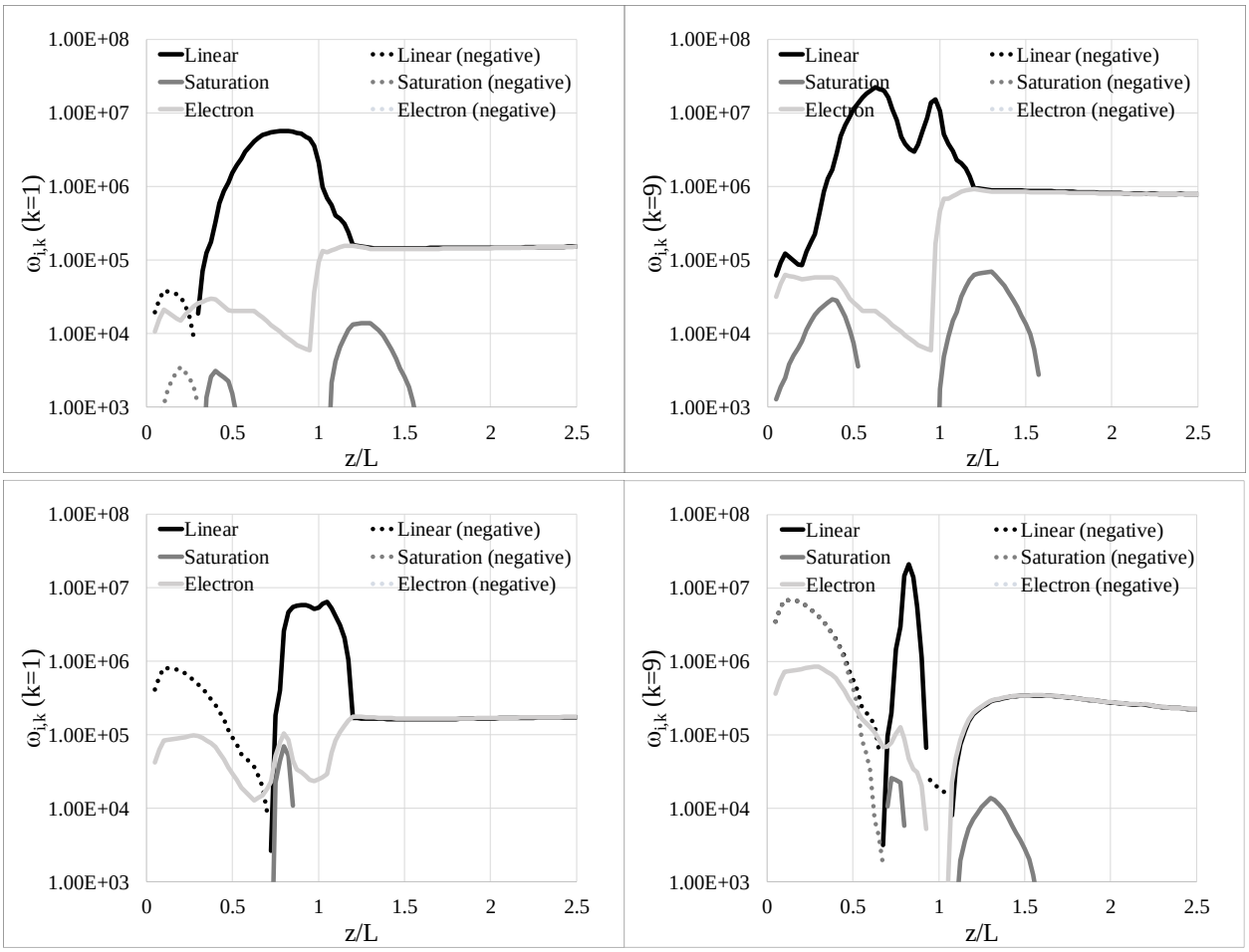

Figure 4. Values of the imaginary part of the wave frequency according to linear theory, $\omega_{i,k,linear}$ (28), and considering saturation, $\omega_{i,k,sat}$ (28). Also shown is the electron contribution to the growth rate as $\omega_{ie,non-linear} = (1-f)\omega_{ie} + f(\omega_{i,k,sat} - \omega_{ii})$ in Eq. (41). First row: cold-ions simulation, second row: warm-ions simulation.

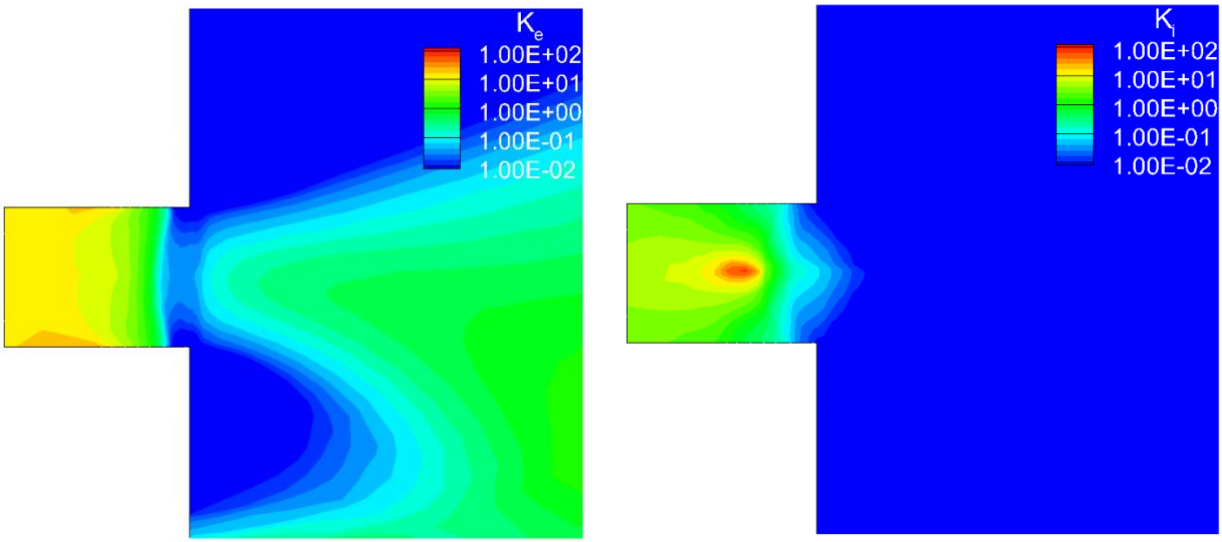

Figure 5. 2-D contour plot of K_e (49) and K_i (47) (non-dimensional thermal equilibration values for electron and ions, respectively) for the warm-ions simulation.

B. Anomalous collision frequency

The anomalous collision frequency is proportional to the sum of the product of the wave action and the non-linear contribution of the electrons to the imaginary part of the wave frequency for all wavenumbers. The values of these variables along the centerline were shown in Subsection IV B. In the first row of Fig. 6, we show the total anomalous collision frequency and the contributions of select wavenumbers for the cold- and warm-ions simulations. The latter has been scaled by 1/N to avoid superimposing the contributions of each wave number with the total anomalous collision frequency. The anomalous collision frequency is compared to the classical collision frequencies between electrons and ions, and electrons and neutrals in the plots of the second row. We observe many qualitative similarities between the results for cold and warm ions, the most notable being a significant decrease in the anomalous collision frequency immediately upstream of the channel exit. This feature is extremely important as it defines the location of the acceleration region (see Fig. (1)). Downstream of the channel exit, the value of the anomalous collision frequency increases with the electron contribution to the imaginary part of the wave frequency, which approaches the linear theory result when f=0. In Fig. 4, the difference in values of $\omega_{ie,non-linear}$ is smaller than the difference between values of the anomalous collision frequency between the acceleration and plume regions. This is due to the $|\mathbf{u}_e - \mathbf{u}_i|$ term in the denominator of (41). The latter becomes larger in the acceleration region as the electron drift increases with the Hall parameter, which in turn increases for lower values of the anomalous collision frequency.

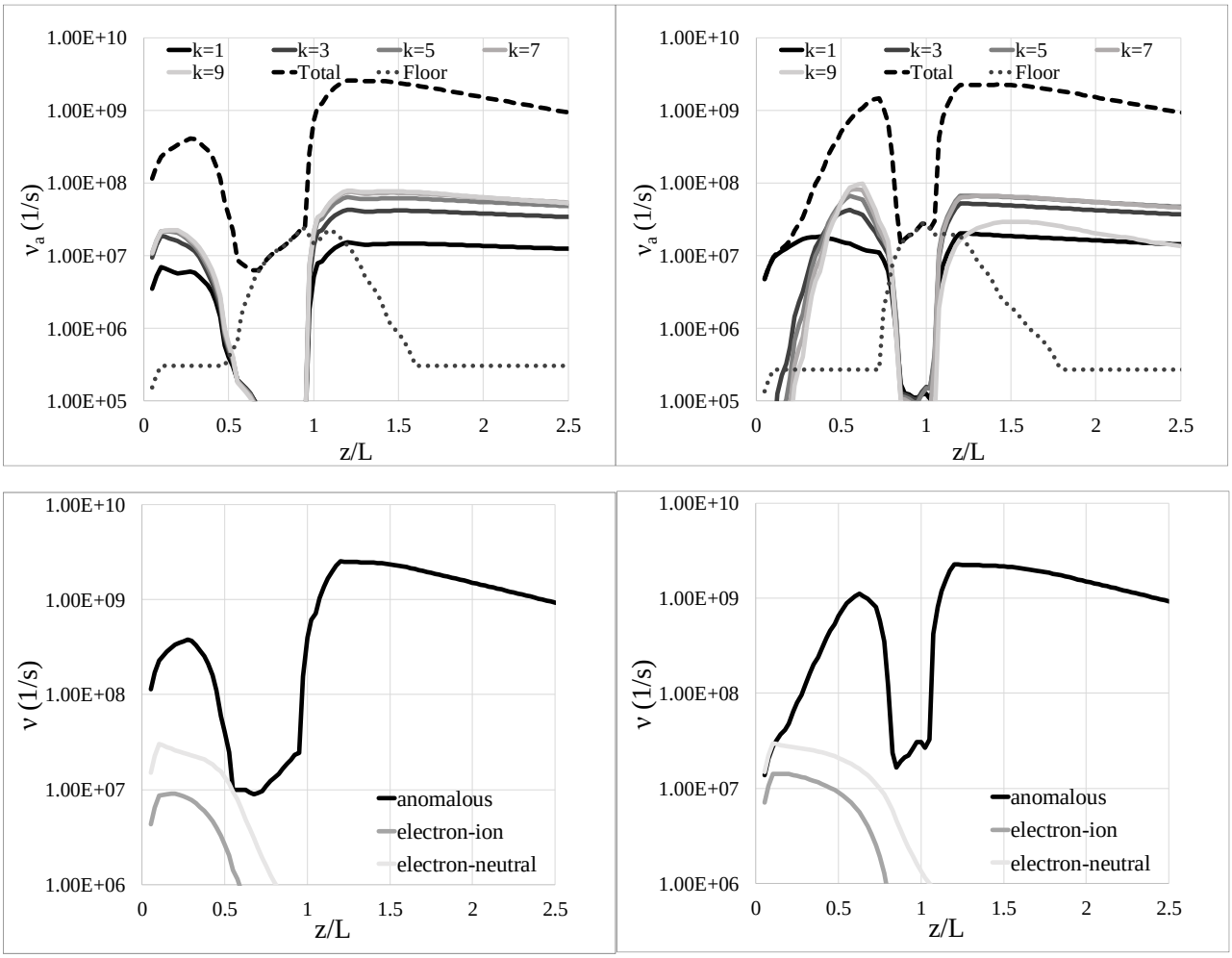

Figure 6. First row: Distribution of the anomalous collision along the channel centerline and contribution of each individual wave numbers for cold-ions (left) and warm-ions (right) simulations. Second row: comparison between anomalous collision frequency and classical collision frequencies for cold-ions (left) and warm-ions (right) simulations.

Differences between the cold-ions and warm-ions simulations are more noticeable inside the channel. This was expected as Landau damping affects primarily the ionization region (z/L<0.6). For cold ions, the wave action is saturated everywhere along the channel centerline. Note that there exists a fundamental inconsistency in our simulations with cold ions, since our simulations predict saturation due to ion trapping everywhere yet we maintain the ion temperature cold. Thus, the shape of the anomalous collision frequency is determined by $\omega_{ie,non-linear} \approx \nu_{in}/2$ inside the channel. ν_{in} is a function of the neutral density that decreases monotonically for z/L>0.25. The anomalous collision frequency decays in consequence downstream of z/L>0.25. The warm-ions simulation is more complex to analyze inside the channel, as the wave action is not always saturated and $\omega_{ie,non-linear}$ depends on Landau damping when f~1. For warm ions, the anomalous collision frequency at the anode is lower than for cold ions as the wave action is negligible for all wavenumbers except for the first. In the first half of the channel, the rate of growth of the wave action is faster than the rate of decrease of $\omega_{ie,non-linear}$. This occurs as the effect of Landau damping becomes less important downstream in the channel. Thus, the anomalous collision frequency follows a trend similar to the wave action, with a rapid increase as we move downstream in the channel. After the wave action reaches saturation (between z/L=0.5 and z/L=0.7, depending on the wave number (see Fig. 2)), the behavior of the anomalous collision frequency is controlled by $\omega_{ie,non-linear}$ as in the cold-ions case. When the wave action reaches saturation, our results for warm ions run into the same inconsistency that was previously noted for cold ions: ion trapping has been considered as the saturation mechanism but the ions remain relatively cold (albeit warmer than in the cold-ions simulation). However, this only occurs for a very narrow region immediately upstream of the acceleration region.

The floor anomalous collision frequency (43) controls the maximum resistivity value that can be achieved before the electrons drift exceeds the thermal velocity. It is shown in Fig. 6 that the floor anomalous collision frequency is higher than the anomalous collision frequency predicted by (41) in the acceleration region. This is because f=1 in (41), the wave action is at its saturation value, and Landau damping is negligible for the ratio of electron and ion temperatures found in the simulations. Since in the acceleration region, as shown in Fig. 5, neither ions nor electrons obey a Maxwellian distribution, Eq. (41) is no longer valid. If ion trapping is indeed the cause for saturation, $\omega_{ie,non-linear}$ in Eq. (41) could be rewritten in a simplified manner as

$$\omega_{ie,non-linear} = (1-f)\omega_{ie} + f\left(\omega_{i,k,sat} - \omega_{ii} - \omega_{ii,sat}\right). \tag{54}$$

In the acceleration region, this expression becomes $\omega_{ie,non-linear} = -\omega_{ii,sat}$, where the right-hand side accounts for the effect of ions being trapped by the waves. This term is difficult to quantify. Thus, the significance of the floor anomalous collision frequency in the acceleration region is that it accounts for physical phenomena that is not yet completely understood.

The second row in Fig. 6 shows a comparison between the anomalous collision frequency computed with the first-principles model and the classical collision frequencies due to electron collisions with ions and neutrals. We find that the ratio between anomalous and classical collision frequency is more than 1000 in the plume. The only location at which the classical collision frequency is comparable to the anomalous is immediately upstream of the acceleration region. The distribution of classical and anomalous collision frequencies along the centerline is comparable to those found in simulations conducted with the experimentally informed profile [20]. In Fig. 7, we show 2-D contour plots of the anomalous collision frequency for the warm-ions simulation that suggest that the distribution of the anomalous collision frequency inside the channel exhibits low dependency on the radial location. In the thruster plume, the wave action is advected with the ion velocity and, in consequence, the anomalous collision frequency follows the expansion of the beam. Finally, we show a contour plot of the two-dimensional cross-field resistivity distribution. The resistivity is obtained from Eq. (33) as the relation between the electric field and the electron current $\mathbf{j}_e$=-e$n_0\mathbf{u}_e$ across magnetic field lines, and takes the form

$$\eta = \frac{m_e\left(\nu_{ei}+\nu_{en}+\nu_a\right)}{e^2 n_0}\left(1+\Omega_e^2\right), \quad \Omega_e = \frac{eB}{m_e\left(\nu_{ei}+\nu_{en}+\nu_a\right)}. \tag{55}$$

As expected by the large plasma potential gradients found in the acceleration region, the cross-field resistivity is largest around z/L=1 and decreases rapidly in the ionization and plume regions, which exhibit small changes in the plasma potential. The resistivity values found in our simulations compare qualitatively well with the mobility (inverse resistivity) found by LaFleur [29] with a theoretical model also based on wave saturation due to ion trapping. However,

the results in [29] were obtained for a different thruster and using a fixed plasma solution rather than a fully self-consistent solution in which the plasma adjusts to changes in the resistivity.

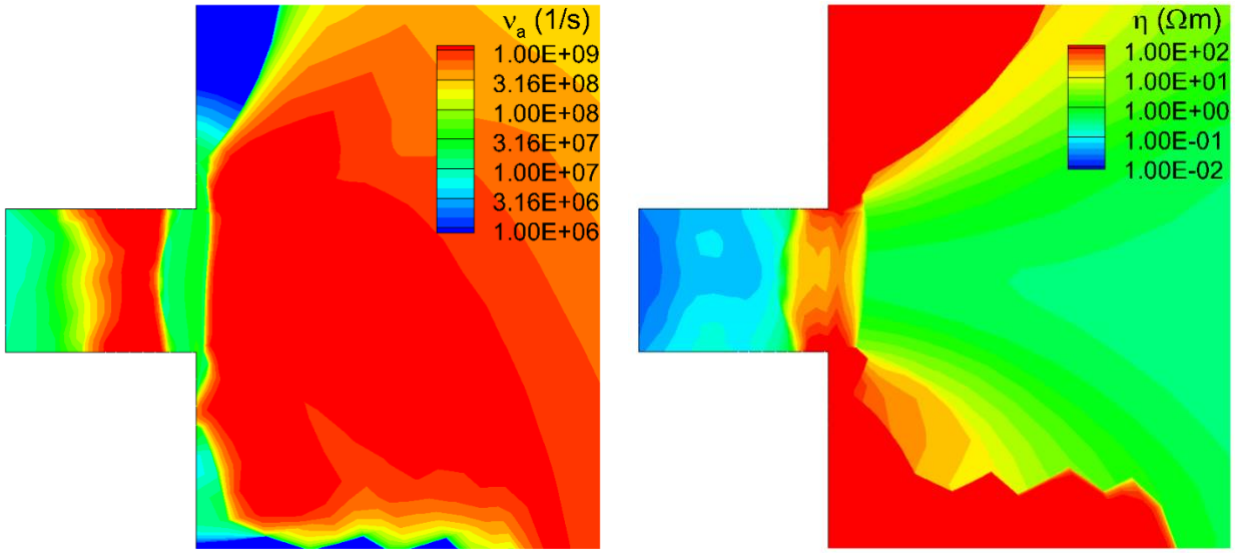

Figure 7. 2-D contour plots of the anomalous collision frequency (left) and plasma resistivity (right) in the channel and thruster plume for the warm-ions simulation.

C. Plasma properties and comparison with experimentally informed profile

In this subsection, we compare the results of our first-principles simulations to those of numerical simulations conducted with an experimentally informed anomalous collision frequency profile. We also depict comparisons with experimental measurements when available. Experimental measurements were obtained using wall and fast scanning injected probes. Electron temperature measurements at the channel walls have been extrapolated to the channel centerline assuming isothermal B-lines [32]. Injected probes are known to perturb the plasma upstream of the peak magnetic field [33] and, in consequence, only measurements in the plume are shown. We observe that the difference in the location of the acceleration region between first-principles simulations and the simulation with an experimentally informed anomalous collision frequency profile is approximately 10% of the acceleration channel. The warm-ions simulation predicts the acceleration region to be downstream because the high resistivity region starts at z/L=0.8 while it starts at z/L=0.7 in the experimentally informed simulation, and z/L=0.6 for the simulation with cold ions. The reason for the late increase in resistivity for the warm-ions simulation is that, when Landau damping is not negligible, the wave action for high wavenumbers reaches saturation at a more downstream location (Fig. 2). Another consequence of the downstream location is the electron temperature being also downstream of the location suggested by the measurements and achieving a higher peak value. The latter can be explained due to heat losses to the walls being very small for z/L>1. As the electron temperature profile moves downstream, a larger portion of the high temperature region falls outside of the channel. Finally, the first-principles simulations exhibit higher values of the plasma density inside the channel than the simulation informed by experimental measurements. This is a consequence of the anomalous collision frequency being higher than the experimentally informed profile for z/L<0.5 in both first-principles simulations. Even though very small differences can be observed in Fig. 8 between the plasma potential profiles of the three simulations upstream of the acceleration region (a result consistent with the study shown in Fig. 1), higher anomalous collision frequency values in the ionization region lead to lower cross-field resistivity. For the same amount of anode current, the plasma potential profile will be flatter with reduced resistivity. Differences in the plasma potential profile in the ionization region are hard to observe in Fig. 8 because gradients in the acceleration region are much larger. However, the flatter plasma potential profile in the ionization region found in first-principles simulations results in stagnation of the ions and higher densities. Since no experimental measurements of the plasma density exist, we cannot draw a conclusion on whether the first-principles simulation are able to reproduce the plasma conditions in the ionization region of the Hall thruster.

With respect to performance comparisons, we cannot directly compare the results of the first-principles simulations with experimental measurements since only singly charged ions were considered in the simulations. The measured thrust was 400 mN at nominal operating conditions (300 V – 20 A). The cold-ions and warm-ions simulations yielded, respectively, 362 and 325 mN. Overall, the cold-ions simulation appears to offer a better comparison with plasma and performance measurements. However, the warm-ions simulation accounts for physical phenomena that are not considered in the cold-ions simulation. The reason for the warm-ions simulations yielding worse agreement with experimental measurements may lie in the exponential sensitivity of Landau damping to the ratio between electron and ion temperatures. For instance, the Landau damping term decreases by more than an order of magnitude between $T_e/T_i = 10$ and $T_e/T_i = 15$. These ratios are common in the discharge channel. By eliminating the Landau damping effect in the cold-ions simulation, we simplified the physics model and eliminated the largest sensitivity of the simulation to the ion temperature. In addition, it was shown that the acceleration region moves downstream in the warm ions simulation because the wave action saturates more downstream along the channel with increasing wavenumbers. The simplified model for the wave action (28) may not capture with complete fidelity the physics of the transition between linear growth and saturation and, close to saturation, Eq. (54) may be valid instead of (41). In consequence, the exact location at which the wave action saturates for each wavenumber may not be captured with enough precision in our simulations.

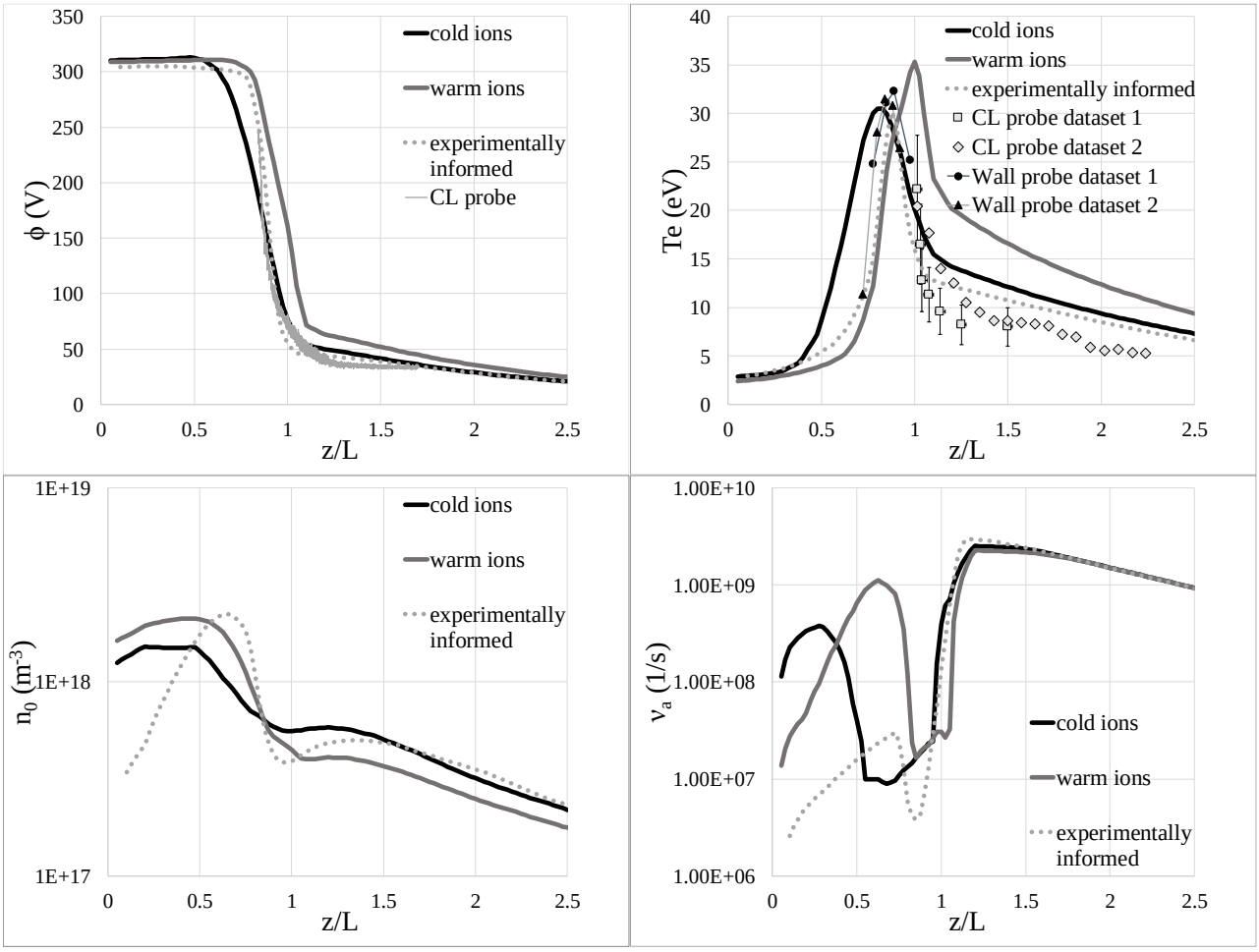

Figure 8. Comparison between plasma properties along the centerline for first-principles simulations and Hall2De simulation with experimentally informed anomalous collision frequency profile. Experimental results are shown when available. Upper-left: plasma potential, upper-right: electron temperature, bottom-left: plasma density, bottom-right: anomalous collision frequency

V.Discussion: what does the first-principles model teach us about anomalous transport in Hall thrusters?

We have developed a numerical model for the cross-field anomalous transport in Hall thrusters that provides self-consistent, stable solutions that agree reasonably well with experimental measurements. This allows us to postulate some hypothesis about the physical mechanisms that control the anomalous transport. The overarching conclusion is that the electron cyclotron drift instability (ECDI), combined with a saturation mechanism, such as ion trapping, can explain the presence of enhanced cross-field anomalous transport for electrons. Confirmation of the role of the ECDI in the anomalous electron transport and the presence of saturation mechanisms such as ion trapping must come from direct experimental measurements of the waves and detailed kinetic simulations that could self-consistently capture the distribution functions of the species in the plasma. The most important ingredient in our model is that the relation between the amplitude of the waves (accounted for by the wave action) and the anomalous collision frequency is dependent on the shape of the electron distribution function (41). Since the electrons move from the thruster plume to the anode and the instability is advected with the ion velocity in the opposite direction, we will describe first conclusions that can be drawn about the behavior of the electrons following their path from the plume to the anode. This will be followed by a description of the evolution of the instability and the ions in the opposite direction.

A. Electrons

In the plume region, the electrons follow a Maxwellian distribution and are isothermal, according to the large value of K_e (49) found in the plume (Fig. 5). In the cathode region, anomalous resistivity does not have an effect. As the electrons start interacting with the ion beam, which advects the wave energy into the plume, the electrons provide some energy to the wave that keeps the latter saturated. This is because $\omega_{ie,non-linear} = \omega_{ie}$ in this region. At the same time, we find that the relationship between the wave action and the anomalous force is also proportional to ω_{ie}, allowing the electrons to find a path with very low resistivity between the cathode plume and the thruster channel.

In the acceleration region, electrons do not obey a Maxwellian distribution function. Due to the large azimuthal electron drift velocity, we find large differences between the energy of the ions in the azimuthal and axial directions. The latter has also been observed in PIC simulations [18]. The consequence of this phenomenon in our model is that the electrons do not contribute as much as they did in the plume region to the growth rate of the wave. Since we do not find any mechanism in our simulations that could contribute to the damping of the wave action in the acceleration region, the contribution of the electrons to the growth rate must be minimal in order to maintain saturation. It is possible though that, in reality, non-linear mechanisms associated with ion trapping (54) or any other saturation mechanism may balance the contribution of the electrons. Damping due to non-linear effects is difficult to quantify theoretically. The physics of the acceleration region can also be explained in terms of transfer of energy between the electrons and the wave. In the linear stage of the ECDI, the electrons lose momentum in the azimuthal direction, which results in turn in growth of the waves. A consequence of losing momentum in the azimuthal direction is an increase in the cross-field electron mobility due to the coupling of the cross-field and azimuthal directions in Ohm's law. Thus, if the electrons in the acceleration region do not lose as much momentum in the azimuthal direction as they would if they were Maxwellian, the cross-field transport is also less enhanced, leading to higher values of the resistivity of the plasma.

In the ionization region, K_e is large, which means in principle that electrons are thermalized and $\omega_{ie,non-linear} = \omega_{ie}$ could be employed. However, in this region the ions are also Maxwellian, based on the values of K_i (Fig. 5) and we chose to use $\omega_{ie,non-linear}$ with f=1. This was motivated by the fact that $\omega_{ie,non-linear} = \omega_{i,k,sat} - \omega_{ii}$ must always be true if ions are Maxwellian. For f=1, $\omega_{ie,non-linear}$ is minimum, which in turn results in the lowest possible proportionality factor between the anomalous collision frequency and the wave action. Thus, we encounter some open questions about the electron behavior in the ionization region. It may be possible that, even when K_e is large, electrons that come from the acceleration region need more time for equilibration with electrons generated in the channel due to interactions with the waves. Another possibility is that ions, which can be trapped by the waves at saturation, do not follow a Maxwellian distribution even in regions where K_i (which does not account for wave interactions) is large. Since LIF measurements of the ions in the ionization region does not suggest that ion trapping is significant in the ionization region [26], the physics of the ionization region merit further investigation. Two major difficulties in understanding the anomalous transport in the ionization region are that large variations in the anomalous collision frequency lead to changes in the plasma potential that are within the experimental uncertainty of measurements (Fig. 1) and that the effect of Landau damping is highly sensitive to the ratio of electron and ion temperatures.

B. Waves and ions

In the ionization region, the balance between Landau damping and growth due to electron drift controls the behavior of the wave action. Landau damping decreases as the electron temperature increases. In consequence, at the downstream end of the ionization region, Landau damping becomes negligible. It is shown in the simulations that the very large electron drift in the azimuthal direction is not required for the waves to saturate. Saturation is achieved before the region of steepest plasma potential gradients. This is due to the advection term in the wave action equation (26) being small as ion velocities are close to stagnation immediately upstream of the acceleration region. Thus, as the contribution of the electron drift to the growth rate becomes larger than Landau damping, the wave action increases quasi-exponentially.

In the acceleration region, the steep plasma potential rapidly increases the ion velocity. New ions generated in this region by ionization or charge-exchange have much lower velocities than those that are generated in the ionization region and do not equilibrate. Thus, neither electrons nor ions are Maxwellian in the acceleration region. Ion trapping may also be possible as waves reach saturation. Even though the expression for Landau damping in (24) assumes Maxwellian ions, we argue that Landau damping still has to depend on the ratio between electron and ion temperatures. Since the value of the electron temperature reaches its maximum in the acceleration region, we conclude that neglecting the effect of linear Landau damping in the acceleration region is a reasonable approximation. However, as noted above, damping due to non-linear effects may exist (54).

Since we cannot model the particularities of the acceleration region, our model relies heavily on the floor anomalous collision frequency. According to (41), $\omega_{ie,non-linear} \approx 0$ and, in consequence, $\nu_a \approx 0$ regardless of the wave action. This solution works well in the H6 thruster because the acceleration region is very steep (in the experimentally informed solution, the drift velocity is approximately equal to the thermal velocity at the steepest point of the acceleration region). Even though this model has not been tested for other thrusters or operating conditions, we have found smoother acceleration regions than that of the H6 in some of our previous investigations. Thus, a model based on limiting the anomalous collision frequency in a way such that the drift does not exceed the thermal velocity may not accurately reproduce the behavior of thrusters for which $|\mathbf{u_e}|$ is considerably smaller than v_{te} in the acceleration region (i.e., a ratio of 0.5 or less). While the latter will be the subject of future investigations, a possible manner in which the presented model can adapt to this situation is by predicting smaller deviations from the Maxwellian distribution function for the electrons (i.e., $\omega_{ie,non-linear}$ becoming larger in the acceleration region). Another possibility for increasing $\omega_{ie,non-linear}$ is to find a model for $\omega_{ii,sat}$ in the acceleration region.

In the plume region, multiple ion populations exist. Ions that generated in the ionization region, the acceleration region, and the plume are present. These populations do not necessarily need to be Maxwellian. For instance, the equilibration length for ions generated in the ionization region is large due to their velocity. Ions generated in the acceleration region and plume ions may not be numerous enough to be considered collisional and can have a wide range of energies. Thus, we cannot directly derive an expression for the contribution of the ions to the imaginary part of the wave frequency. However, we can use the same approach applied to the situation in which electrons are not Maxwellian to write

$$\omega_{ii,plume} = \omega_{ii} + \omega_{ii,sat} = \left(\omega_{i,k,sat} - \omega_{ie}\right) \approx -\omega_{ie}\,, \tag{56}$$

with ω_{ie} from (24). That linear and non-linear effects balance the contribution of the electrons, ω_{ie}, is plausible since Landau damping should increase with the lower electron temperatures found in the plume. In addition, non-linear effects, such as ion trapping, can also contribute to $\omega_{ii,plume}$. Finally, it is worth exploring the hypothesis formulated in [28] that postulated that the different populations in the plume interact differently with the waves, according to their average velocity and temperature.

C. Future work

While the presented model has shown potential for achieving the main objective of our investigation: "*to produce a first-principles model that could self-consistently predict the distribution of anomalous collision frequency in Hall2De simulations"*, we still need to show that it can be satisfactorily applied to other thrusters (including magnetically shielded thrusters [32]) and operating conditions. In addition, the model should be able to reproduce certain trends observed in experiments, such as axial shifts in the location of the acceleration region with discharge voltage and magnetic field magnitude [34-35].

Future topics of investigation should also be focused on the physical mechanisms that our model cannot self-consistently explain. Deviations from linear theory are captured using approximations, such as assuming that the

saturation depends linearly on the ratio of the wave action and its saturation value, and must be confirmed by other means. We also found a manner to circumvent the need of determining non-Maxwellian distribution functions with the use of Eqs. (41) and (56). This approach requires that at least one of the species be Maxwellian and fails in the acceleration region, where the anomalous collision frequency is limited by its floor value. Our results show that the anomalous collision frequency in the acceleration region cannot be related to the wave energy the way linear theory predicts (38). A non-linear mechanism must be present in order to avoid maximum mobility values in the locations where linear theory predicts maximum growth rates. Even though we have assumed saturation due to ion trapping in our model, this phenomenon has not been experimentally observed in Hall thrusters. Eq. (28) is general enough that this numerical model can be used to test alternative saturation mechanisms. Detailed numerical investigations of the physics of the acceleration region will require the use of experimental techniques and kinetic computational methods.

VI.Conclusion

We presented a computational model based on the hypothesis that the anomalous electron mobility across magnetic field lines observed in Hall thrusters is due to the growth and eventual saturation of the electron cyclotron drift instability. This approach contrasts with our previous investigations [22, 25, 28], which heavily relied on linear ion-acoustic theory. The use of linear theory for describing anomalous transport in a Hall thruster is not appropriate, as it will predict large mobility in regions where the electric field is large, but an increase in mobility will in turn translate into lower electric fields for a fixed electron current. Thus, linear theory of the ion-acoustic instability cannot capture self-consistently the electrostatic forces that drives the evolution of the ions in the acceleration region of Hall thrusters. By accounting for saturation of the instability, we effectively modify the relation between the cross-field transport and the electron drift, increasing the resistivity in the acceleration region.

The first-principles model for saturation of the electron cyclotron drift instability presented in this article solves a set of equations that describe the evolution of the wave action (a measure of the amplitude of the waves in the instability) as a function of the wavenumber. These equations take the form of a system of hyperbolic partial differential equations in which the wave action is advected by the ion velocity and grows or decays according to a source (or sink) term on the right-hand side of the equation. Each of the equations can be solved independently of one another and concurrently with the hydrodynamics equations in Hall2De. The cost of solving this system of equations is comparable to the cost of solving the equations that describe the motion of the ions at each time-step. The anomalous collision frequency can be recovered as the sum for all wavenumbers of the product of the wave action and the contribution of the electrons to the growth rate of the waves. For linear theory, the latter is proportional to the electron drift velocity. In our model, we evaluate the thermalization time of ions and electrons to determine whether to apply linear or non-linear theory.

Comparison of the results of our first-principles model with experimental measurements for the H6 thruster operating at nominal conditions (300 V – 20 A) reveals that simulations are able to predict the location of the acceleration region with an error that is less than 10% of the acceleration channel length. Our simulations also suggest that in the acceleration region, neither ions nor electrons follow a Maxwellian distribution function. In this case, the anomalous collision frequency approaches zero and its value is controlled by a floor value that prevents the drift velocity of the ions from exceeding the thermal velocity. We also found that linear Landau damping, a mechanism that reduces the wave action as the ion temperature increases is only important in the ionization region, where plasma parameters such as the plasma potential exhibit very low sensitivity to the anomalous collision frequency.

Limitations of the presented model are acknowledged in the sense that the exact distribution functions when deviations from the thermalized distribution occur cannot be recovered. Their effect on the anomalous collision frequency is rather reconstructed from other quantities that remain known. Full kinetic simulations with computation times much longer than the typical runtime of Hall2De may be necessary to determine the fine details of the physics that govern cross-field transport in Hall thrusters. The validity of the model must be further assessed by applying it to simulations of other thrusters and/or operating conditions.

Acknowledgments

The authors would like to acknowledge the contributions of Dr. Ioannis G. Mikellides and Prof. Benjamin A. Jorns, whose work set the foundations for the model presented in this article. The research described in this paper was carried out by the Jet Propulsion Laboratory, California Institute of Technology, under a contract with the National Aeronautics and Space Administration. The support of the joint NASA GRC and JPL development of the Advanced Electric Propulsion System by NASA's Space Technology Mission Directorate through the Solar Electric Propulsion Technology Demonstration Mission project is gratefully acknowledged.

References

[1] Brophy, J. R., and Friedman, L., "Returning an Entire Near-Earth Asteroid in Support of Human Exploration Beyond Low-Earth Orbit," in IAF Global Exploration Conference, Washington, D. C., 2012.

[2] Brophy, J. R., Friedman, L., and Culick, F., "Asteroid Retrieval Feasibility," in Aerospace Conference, 2012, Big Sky, MT, 2012, pp. 1 - 16.

[3] Brophy, J. R., and Oleson, S., "Spacecraft Conceptual Design for Returning Entire Near-Earth Asteroids", AIAA paper 2012-4067, July 2012.

[4] Elkins-Tanton, L. T., Asphaug, E., Bell, J., Bercovici, D., Bills, B. G., Binzel, R. P., Bottke, W. F., Jun, I., Marchi, S., Oh, D., Polanskey, C. A., Weiss, B. P., Wenkert, D., and Zuber, M. T., "Journey to a Metal World: Concept for a Discovery Mission to Psyche", 45th Lunar and Planetary Science Conference, 2014.

[5] Hirakawa, M., and Arakawa, Y., "Numerical Simulation of Plasma Particle Behavior in a Hall Thruster", AIAA paper 96-3195, July, 1996.

[6] Adam, J. C., Heron, A., and Laval, G., "Study of Stationary Plasma Thrusters Using Two-dimensional Fully Kinetic Simulations", Physics of Plasmas, Vol. 11, 2004, 295, doi: 10.1063/1.1632904

[7] Szabo, J. J., "Fully kinetic numerical modeling of a plasma thruster", Ph.D. thesis, Massachusetts Institute of Technology, 2001.

[8] Heron, A., and Adam, J. C., "Anomalous Conductivity in Hall Thrusters: Effects of the Non-linear Coupling of the Electron-Cyclotron Drift Instability with Secondary Electron Emission of the Walls", *Physics of Plasmas*, Vol. 20, 082313, 2013, doi: 10.1063/1.4818796

[9] Coche, P. and Garrigues, L., "A Two-Dimensional (Azimuthal-Axial) Particle-In-Cell Model of a Hall Thruster", Phys Plamas 21, 023503, 2014, doi: 10.1063/1.4864625

[10] Forslund, D. W., Morse, R. L., and Nielson, C. W., "Electron Cyclotron Drift Instability," *Physical Review Letters*, Vol. 25, no. 18, pp. 1266, 1970, doi: 10.1103/PhysRevLett.25.1266

[11] Bychenkov, V. Y., Silin, V. P., and Uryupin, S. A., "Ion-acoustic Turbulence and Anomalous Transport", *Physics Reports*, Vol. 164, Issue 3, 1988, 199-215, doi: 10.1016/0370-1573(90)90122-I

[12] de Kluvier, H., Perepelkin, N. F., and Hirose, A., "Experimental Results on Current-driven Turbulent Plasmas – a Survey", *Physics Reports*, Vol. 199, Issue 6, 1991, 281-381, doi: 10.1016/0370-1573(91)90060-Y

[13] Stix, T. H., *Waves in Plasmas*, Springer-Verlag, New York, 1992.

[14] Horton, H., *Turbulent transport in magnetized plasmas*, World Scientific, Singapore, 2012.

[15] Tsikata, S., Lemoine, N., Pisarev, V., and Gresillon, D. M., "Dispersion Relation of Electron Density Fluctuations in a Hall Thruster Plasma, Observed by Collective Light Scattering", *Physics of Plasmas*, Vol. 16(3), 033506, 2009, doi: 10.1063/1.3093261

[16] Cavalier, J., Lemoine, N., Bonhomme, G., Tsikata, S., Honore, C., and Gresillon, D., "Hall Thruster Plasma Fluctuations Identified as the ExB Electron Drift Instability: Modeling and Fitting on Experimental data", *Physics of Plasmas*, Vol. 20, 082107, 2013, doi: 10.1063/1.4817743.

[17] Ducrocq, A., Adam, J. C., Heron, A., and Laval, G., "High-Frequency Electron Drift Instability in the Cross-Field Configuration of Hall Thrusters", *Physics of Plasmas*, Vol. 13(10), 102111, 2006, doi: 10.1063/1.2359718.

[18] Lafleur, T., Baalrud, S. D., and Chabert, P.," Theory for the Anomalous Electron Transport in Hall Effect Thrusters. I. Insights from Particle-In-Cell Simulations", *Physics of Plasmas*, Vol. 23, 053502, 2016, doi: 10.1063/1.4948495

[19] Mikellides, I. G. and Katz, I., "Numerical Simulations of Hall-effect Plasma Accelerators on a Magnetic-Field-Aligned Mesh", Physical Review E, Vol. 86, 2012, p. 046703, doi: 10.1103/PhysRevE.86.046703

[20] Lopez Ortega, A. and Mikellides, I. G., "The Importance of the Cathode Plume and its Interactions with the Ion Beam in Numerical Simulations of Hall Thrusters", *Physics of Plasmas*, Vol. 23, 043515, 2016, doi: 10.1063/1.4947554

[21] Katz, I. and Mikellides, I. G., "Neutral gas free molecular flow algorithm including ionization and walls for use in plasma simulations", *Journal of Computational Physics*, Vol. 230, 2011, pp. 1454-1464, doi: 10.1016/j.jcp.2010.11.013

[22] Katz, I., Mikellides, I. G., Jorns, B. A., and López Ortega, A., "Hall2De Simulations with an Anomalous Transport Model Based on the Electron Cyclotron Drift Instability", IEPC paper 2015-402, July, 2015.

[23] Lopez Ortega, A., Mikellides, I. G., and Jorns, B. A., "First-principles Modeling of IAT-driven Anomalous Resistivity in Hollow Cathode Discharges II: Numerical Simulations and Comparisons with Experiments", AIAA paper No. 2016-4627, July 2016.

[24] Lopez Ortega, A., Mikellides, I. G., and Jorns, B. A., "Hollow Cathode Plasma Simulations with a First-principles Model of IAT-driven Anomalous Resistivity", submitted to *Journal of Propulsion and Power*, 2017.

[25] Mikellides, I. G., Lopez Ortega, A., Katz, I., and Jorns, B. A., "Hall2De Simulations with a First-principles Electron Transport Model Based on the Electron Cyclotron Drift Instability", AIAA paper 2016-4618, July 2016.

[26] Huang, W., Reid, B. M., Smith, T. B., and Gallimore, A. D., "Laser-Induced Fluorescence of Singly-Charged Xenon in a 6-kW Hall Thruster plume", AIAA paper 2009-5355, August 2009.

[27] Huang, H. *Study of Hall Thruster Discharge Channel Wall Erosion via Optical Diagnostics*, Phd. Thesis, University of Michigan, 2011.

[28] Katz, I., Lopez Ortega, A., Jorns, B. A., and Mikellides, I. G., "Growth and Saturation of Ion Acoustic Waves in Hall Thrusters", AIAA paper 2016-4534, July 2016.

[29] Lafleur, T., Baalrud, S. D., and Chabert, P., "Theory for the Anomalous Electron Transport in Hall Effect Thrusters. II. Kinetic Model", *Physics of Plasmas*, Vol. 23, 053503, 2016, doi: 10.1063/1.4948496

[30] Reid, B. M., "The Influence of Neutral Flow Rate in the Operation of Hall Thrusters," Ph.D. Thesis, Aerospace Engineering, University of Michigan, 2009.

[31] Brown, D. L., Larson, C. W., Haas, J. M., and Gallimore, A. D., "Analytical Extraction of Plasma Properties Using a Hall Thruster Efficiency Architecture", IEPC paper 2007-188, in proceedings of the 30th International Electric Propulsion Conference, Florence, Italy, 2007.

[32] Mikellides, I. G., Katz, I., Hofer, R. R., and Goebel, D. M., "Magnetic Shielding of a Laboratory Hall Thruster. I: Theory and Validation," *Journal of Applied Physics*, Vol. 115, 2014, pp. 043303 (1-20), doi: 10.1063/1.4862313

[33] Jorns, B. A., Goebel, D. M., and Hofer, R. R., "Plasma Perturbations in High-Speed Probing of Hall Thruster Discharge Chambers: Quantification and Mitigation", AIAA paper 2015-4006, July 2015.

[34] Lopez Ortega, A., Mikellides, I. G., and Chaplin, V. H., "Simulations for the Assessment of Pole Erosion in the 12.5-kW Hall Effect Rocket with Magnetic Shielding", IEPC-2017-154, October 2017.

[35] Chaplin, V. H., Jorns, B. A., Conversano, R. W., Lobbia, R. B., and Lopez Ortega, A., "Laser Induced Fluorescence Measurements of the Acceleration Zone in the 12.5 kW HERMeS Hall Thruster", IEPC-2017-229, October 2017.